

### Contents:

- 10 Extrapulmonary Tuberculosis Mimicking Malignancy on  $^{18}\text{F}$  FDG PET/CT Scan: A Case Report  
Arrene Joy B. Baldonado, MD
- 16 Evaluation of Bone Graft Viability Using Three-Phase Bone Scan with Single Photon Emission Tomography (SPECT): A Case Series  
Louen Mark T. Visaya, MD
- 32 Clinical Outcomes of Patients Who Underwent Gallbladder Ultrasound And Cholescintigraphy For Acute Cholecystitis At St. Luke's Medical Center  
Carl Joshua M. Chianpian, MD, Patricia Jarmin L. Pua, MD, Irene S. Bandong, MD
- 40 A Comparative Study of Automated Quantitative and Clinical Visual Analysis of Myocardial Viability among Adult Patients with CAD using Rest-Redistribution Thallium-201 Gated SPECT-MPI  
Mary Amie Gelina E. Dumatol, MD, Angelo O. Martinez, MD, Michele D. Ogbac, MD
- 50 A retrospective study on the concordance of the OSEM and Q.Clear reconstruction algorithms in  $^{18}\text{F}$ -FDG PET-CT imaging of female patients with breast cancer  
Timothy James O. Lam, MD, Sean Ira G. Gacula, MD



# Philippine Journal of Nuclear Medicine

Volume 20 No. 1  
January to June 2025

## Official Publication of the Philippine Society of Nuclear Medicine

The Philippine Journal of Nuclear Medicine is a peer-reviewed journal published by the Philippine Society of Nuclear Medicine. Subscription is free to all PSNM members in good standing as part of their membership privileges.

The Journal will be primarily of interest to medical and paramedical personnel working in nuclear medicine and related fields. Original works in clinical nuclear medicine and allied disciplines in physics, dosimetry, radiation biology, computer science, radiopharmacy, and radiochemistry are welcome. Review articles are usually solicited and published together with related reviews. Case reports of outstanding interest are likewise welcome. PSNM documents and position papers of interest to the reader will also be published as necessary.

Manuscripts for consideration should be sent to:

The Editor, Vincent Peter C. Magboo, MD  
Philippine Journal of Nuclear Medicine  
c/o Philippine Society of Nuclear Medicine  
Unit 209 One Beatriz Tower Condo  
4 Lauan St. cor. Aurora Blvd  
Project 3, Quezon City 1102, Philippines  
Contact. No.: +63 (966) 976 5676  
Email: vcmagboo@up.edu.ph  
philnucmed@gmail.com

All business communications and requests for complimentary copies should be addressed to the above.

Copyright©2025 by the Philippine Society of Nuclear Medicine, Inc. All rights reserved. No part of this work may be reproduced by electronic or

other means, or translated without written permission from the copyright owner. The copyright on articles published by the Philippine Journal of Nuclear Medicine is held by the PSNM, therefore, each author of accepted manuscripts must agree to automatic transfer of the copyright to the publishers. See Information for Authors for further instructions.

The copyright covers the exclusive rights to reproduce and distribute the articles. The publishers reserve the right to make available part or all of the contents of this work on the PSNM website ([www.psnm.ph](http://www.psnm.ph)). Copyright of the contents of the website are likewise held by the PSNM.

ISSN 1655-9266

### **PSNM Publications Committee and PJNM Editorial Staff**

#### *Editor*

Vincent Peter C. Magboo, MD

#### *Associate Editors*

Patricia A. Bautista-Penalosa, MD  
Jeanelle Margareth T. Tang, MD

#### *Editorial Board*

Eric B. Cruz, MD  
Michele A. Duldulao-Ogbac, MD  
Jonas Francisco Y. Santiago, MD  
Asela B. Barroso, MD  
Christopher A.C. Carbonell, MD  
Johann Giovanni P. Mea, MD  
Arnel E. Pauco, MD  
Francis Gerard M. Estrada, MD

# INFORMATION FOR AUTHORS

## EDITORIAL POLICY

The Philippine Journal of Nuclear Medicine is the official peer-reviewed publication of the Philippine Society of Nuclear Medicine. The Journal accepts original articles pertinent to the field of nuclear medicine. Articles may be on any of the following: clinical and basic sciences, case reports, technical notes, special contributions, and editorials.

### Submission of manuscripts

The submitted manuscript package should consist of: (1) the full text (including tables) in Microsoft Word, plain text or ConTeXt document format; and (2) high-resolution JPEG files of all images used in the manuscript. The complete manuscript package may be submitted as a compressed (.ZIP) file by email to philnucmed@gmail.com, or in an optical disc (CD/DVD) and mailed to

The Editor: Philippine Journal of Nuclear Medicine, c/o Philippine Society of Nuclear Medicine, Unit 209 One Beatriz Tower Condo, 4 Luanan St. cor. Aurora Blvd., Project 3, Quezon City 1102, Philippines.

Manuscripts should be accompanied by a cover letter signed by the author responsible for correspondence regarding the manuscript. The cover letter should contain the following statement:

"All copyright ownership is transferred to the Philippine Journal of Nuclear Medicine upon acceptance of the article \_\_\_\_\_. This manuscript has been seen and approved by all the authors. The authors stipulate that the material submitted to the Philippine Journal of Nuclear Medicine is an original work and has not been submitted to another publication for concurrent consideration. Any human and/or animal studies undertaken as part of the research are in compliance with regulations of our institution(s) and with generally accepted guidelines governing such work."

The cover letter should also give any additional information that may be helpful to the Editor. Signed cover letters sent by email should be in PDF format.

### MANUSCRIPT FORMAT

Manuscripts must be written in English, and printed on letter-sized white bond paper, 8.5 in x 11 in (21.6 cm x 27.9 cm). The text should be on one side of the

paper only, single-spaced, with at least 1.5 in (4 cm) margins on all sides. Each of the following sections must begin on separate pages and in the following order: title page, abstract, text, acknowledgments, references, tables (each on a separate page), and legends. Pages should be consecutively numbered beginning with the title page. The first line of paragraphs should be indented by at least five spaces.

### Title page

The title page should include: (1) a concise but informative title; (2) a short running head or footline of no more than 40 characters; (3) a complete byline, with first name, middle initial, and last name of each author and highest academic degrees; (4) the complete affiliation for each author, with the name of departments and institutions to which the work should be attributed; (5) disclaimers, if any; (6) the name, address, and telephone number of the author responsible for correspondence about the manuscript; and (7) the name and address of author to whom reprint requests should be directed.

### Abstract and key words

An abstract of no more than 300 words should state the purpose of the study or investigation, summary of methodology, major findings, and principal conclusions. New and important aspects of the study or observations should be emphasized. No figures, abbreviations or reference citations are to be used in the abstract.

### Text

The text of original scientific and technical articles is usually divided into the following sections: Introduction, Materials and Methods, Results, Discussion, and Summary or Conclusion.

Case reports are divided into the following sections: Introduction, Case Report, Discussion, and Conclusion. They should contain a concise description of one to three patients, emphasizing the nuclear medicine aspects and include methodology, data and correlative studies. Procedures should be described in sufficient detail to allow other investigators to reproduce the results.

Other articles, e.g. review articles, position papers, or editorials, should introduce a problem or question, present evidence, and conclude with an answer. Generally, review articles should have extensive documentation. Literature citations should represent the breadth and depth of the subjects being reviewed. The organization of review articles will depend greatly on the subject matter and material.

Generic names must be used throughout the text. Instruments and radiopharmaceuticals must be identified by manufacturer name and address in parentheses.

## Acknowledgments

Persons or agencies contributing substantially to the work, including any grant support, must be acknowledged.

## References

References must be cited in consecutive numerical order at first mention in the text and designated by the reference number in parentheses. References appearing in a table or figure should be numbered sequentially with those in the text.

The reference list must be numbered consecutively as in the text. The journal follows Index Medicus style for references and abbreviates journal names according to the List of Journals Indexed in Index Medicus. 'Unpublished observations' and 'personal communications' should not be used as references, although written—not verbal—communications may be noted as such in the text. The author is responsible for the accuracy of all references and must verify them against the original document.

For journal articles with six or less authors, all authors must be listed. For those with seven or more authors, only the first three are listed, and "et al." is added to the end of the list.

Seabold JE, Conrad GR, Kimball DA, Ponto JA and Cricker JA. Pitfalls in establishing the diagnosis of deep venous thrombophlebitis by indium-111 platelet scintigraphy. *J Nucl Med* 1988;29:1169–1180.

For book and book chapters:

Williams LJ. Evaluation of parathyroid function. In: Brock LJ, Stein JB, eds. *The parathyroid and its diseases*. 4th ed. New York: Wiley; 1985:196–248.

Goodyear B. Bone marrow transplantation in severe combined immunodeficiency syndrome. In: Gree HJ, Blacksmith R, eds. *Proceedings of the fourth biennial meeting of the International Society of Transplantation*. Houston: International Society of Transplantation; 174: 44–46.

For journal article in electronic format:

Author. Title. Journal name. Online publishing date. Available from: URL address.

## Tables

Each table should be typed double-spaced on a separate page. Do not submit tables as photographs. Tables should be self-explanatory and should supplement, not duplicate, the text. Each table must be cited in consecutive numerical order in the text. Tables should be numbered consecutively with a Roman number following the word TABLE.

## Illustrations

Illustrations should clarify and augment the text. Figures should be sharp and of high quality. Glossy photographs of line drawings rendered professionally on white drawing paper in black India ink, with template or typeset lettering, should be submitted. High quality computer-generated art is also acceptable. Letters, numbers, and symbols should be clear and of sufficient size to retain legibility after reduction.

Each illustration must be numbered and cited in consecutive order in the text. Illustrations should be identified on a gummed label. Legends should be typed double-spaced on a separate page. Figures should be numbered with an Arabic number following the word FIGURE.

## Units of measurement

Use of the International System of Units (SI) is standard. Measurements of length, height, weight, and volume must be reported in metric units. Other measurements must be reported in the units in which they were made. Alternative units (non-SI units) should be added in parentheses by the author, if indicated.

## Abbreviations and symbols

Only standard abbreviations and symbols should be used in the text. At first mention, the complete term, followed by its abbreviations in parentheses, must be used in the text. Standard units of measure should not be expanded at first mention. Consult a style manual, if necessary.

## REVIEW PROCEDURE

Submitted manuscripts are peer-reviewed for originality, significance, adequacy of documentation, reader interest, composition, and adherence to the guidelines. Manuscripts are returned to the author for revision if suggestions and criticisms have been made. All accepted manuscripts are subject to editing for scientific accuracy, clarity, and style.



**PSNM**

**MIDYEAR  
CONVENTION**

**AUGUST 2, 2025 ✦ METRO MANILA**

*Save the date! More details to follow!*

## Message from the President of the Society



*The Philippine Journal of Nuclear Medicine plays a crucial role in advancing the practice of Nuclear Medicine. As a platform for disseminating high-quality research, fostering collaboration, and inspiring innovation, it highlights the pivotal role of research in improving patient care and driving progress in the field.*

*Research remains the cornerstone of growth in Nuclear Medicine. It bridges the gap between basic science and clinical applications, enabling us to refine diagnostic techniques, develop advanced therapeutic strategies, and ultimately provide better outcomes for our patients. As practitioners, we are called to embrace a culture of inquiry and evidence-based practice to ensure we remain at the forefront of medical innovation.*

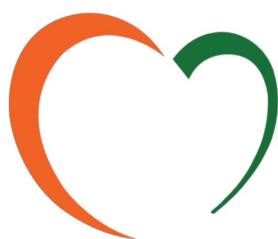
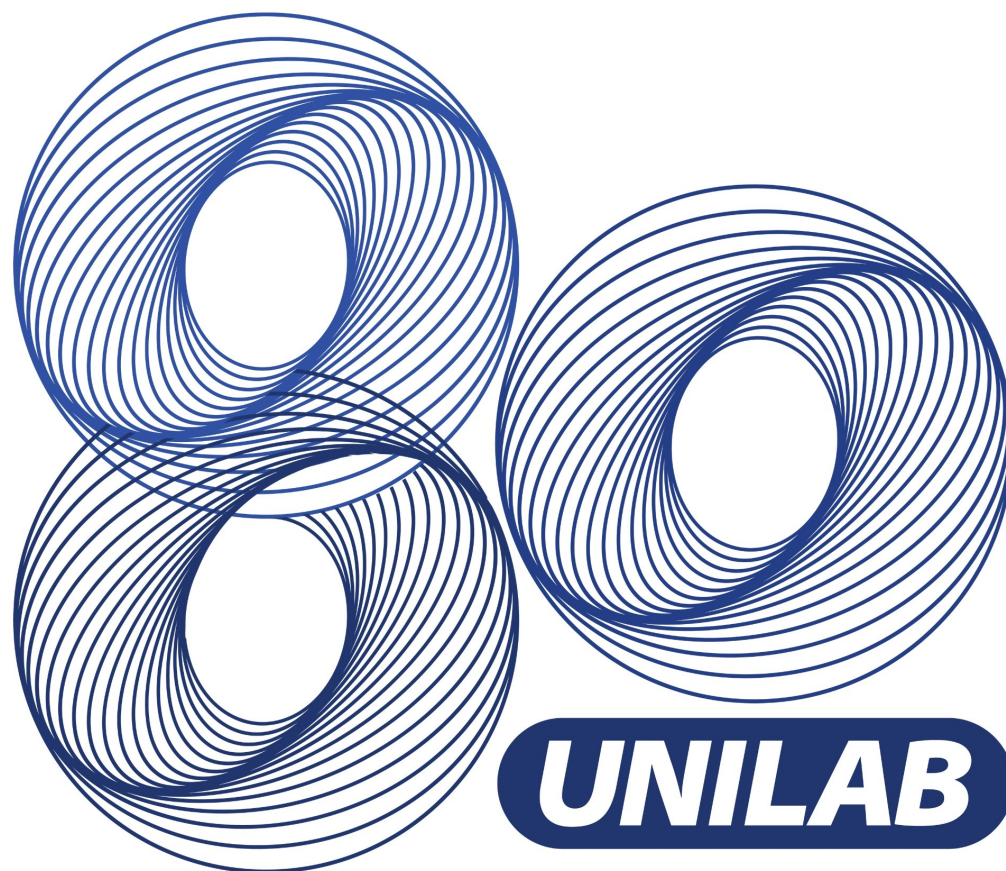
*I extend my heartfelt gratitude to the dedicated editorial team, the contributors who have shared their expertise and findings, and the sponsors who have made this publication possible. Your unwavering support has ensured that the journal continues to serve as an invaluable resource for both the local and international Nuclear Medicine community.*

*As we look ahead, let us strive to foster a spirit of collaboration and innovation. The work we do today lays the groundwork for a brighter future in Nuclear Medicine. Together, let us uphold the highest standards of research and practice for the benefit of our patients and the advancement of our profession.*



**Eric B. Cruz, MD, FPSNM**

*President, Philippine Society of Nuclear Medicine (2023-2025)*



**LRI-THERAPHARMA**

*The Cardio-Metabolic Subsidiaries of UNILAB*

# Levothyroxine

## TFour



*Higher Compliance  
Through Higher Savings*



BRAND	SRP / TAB
TFOUR 50 MCG	₱7.50
BRAND E	₱10.45
28% LOWER IN PRICE THAN BRAND E*	



BRAND	SRP / TAB
TFOUR 100 MCG	₱12.00
BRAND E	₱19.25
38% LOWER IN PRICE THAN BRAND E*	

\*BASED ON PRICES AS OF FEBRUARY 2025\*

# Extrapulmonary Tuberculosis Mimicking Malignancy on $^{18}\text{F}$ FDG PET/CT SCAN: A Case Report

Arrene Joy B. Baldonado, MD

Department of Radiological Sciences, Section of Nuclear Medicine and PET-CT Center, Cardinal Santos Medical Center  
E-mail address: baldonadoarrene@gmail.com

## ABSTRACT

*Extrapulmonary tuberculosis (EPTB) accounts for approximately 15% of TB cases worldwide and often presents with nonspecific signs and symptoms that can closely mimic malignancy. Differentiating EPTB from cancer is challenging, as both conditions may exhibit similar imaging findings. Fluoro-2-deoxyglucose positron emission tomography and computed tomography (FDG PET/CT) is a well-established modality for evaluating malignancies. However, FDG uptake is not exclusive to cancer and can also be observed in inflammatory/infectious conditions, including TB.*

*This report discusses the case of a 29-year-old Filipino male who presented with back pain radiating to the sternal region. A chest CT scan revealed lytic osseous lesions in the ribs, sternum, and vertebrae, along with a lobulated mass in the periportal region. FDG PET/CT was conducted for further assessment, revealing heightened metabolic activity in the aforementioned lesions, which raised concerns for possible malignancy. However, a CT-guided biopsy of the 7th rib revealed caseating granulomatous inflammation consistent with tuberculosis. The patient was treated with a 12-month anti-TB regimen, with follow-up FDG PET/CT demonstrating a favorable response to therapy.*

*This case underscores the importance of considering EPTB in the differential diagnosis of patients with FDG-avid lymphadenopathy and osseous lesions, particularly in endemic regions such as the Philippines. A high index of suspicion, along with histopathologic confirmation, is essential to avoid misdiagnosis and ensure appropriate management.*

**Keywords:** Tuberculosis (TB), Extrapulmonary tuberculosis (EPTB), malignancy, and Fluoro-2- deoxyglucose positron emission tomography and computed tomography (FDG-PET/CT)

## INTRODUCTION

Tuberculosis (TB) remains a significant public health concern in the Philippines, with an incidence of 554 cases per 100,000 people [1]. Caused by *Mycobacterium tuberculosis*, TB primarily affects the lungs but can also involve other organs, leading to extrapulmonary tuberculosis (EPTB) [2]. EPTB accounts for approximately 15% of TB cases worldwide, with lymph node and musculoskeletal TB comprising 30% and 10% of these cases, respectively [2-4]. Unlike pulmonary TB, which presents with respiratory symptoms, EPTB has diverse manifestations that can mimic malignancy, leading to diagnostic delays.

Diagnosing EPTB is complex due to its nonspecific clinical and imaging findings compared to pulmonary TB. CT and MRI are commonly used in malignancy workups, but FDG PET/CT is increasingly utilized for further evaluation.

FDG PET/CT is a nuclear medicine imaging modality frequently used in oncologic evaluations [5]. FDG uptake reflects cellular glycolytic activity, which is elevated not only in malignancies but also in infectious and inflammatory conditions such as TB [5]. This overlap can lead to misdiagnosis, unnecessary procedures, and delayed treatment.

This paper presents a case of EPTB initially suspected of having a malignancy based on chest CT and FDG PET/CT findings.

## Patient Information

A 29-year-old Filipino male complained of back pain radiating to the sternal region with a pain scale of 9/10. There is no associated history of trauma nor any signs and symptoms of chest pain, difficulty breathing, cough, colds, night sweats, fever, or abdominal pain. His past medical history is unremarkable, with no known tuberculosis or human immunodeficiency virus (HIV) infection. Physical examination revealed clear breath sounds and no palpable lymph nodes detected.

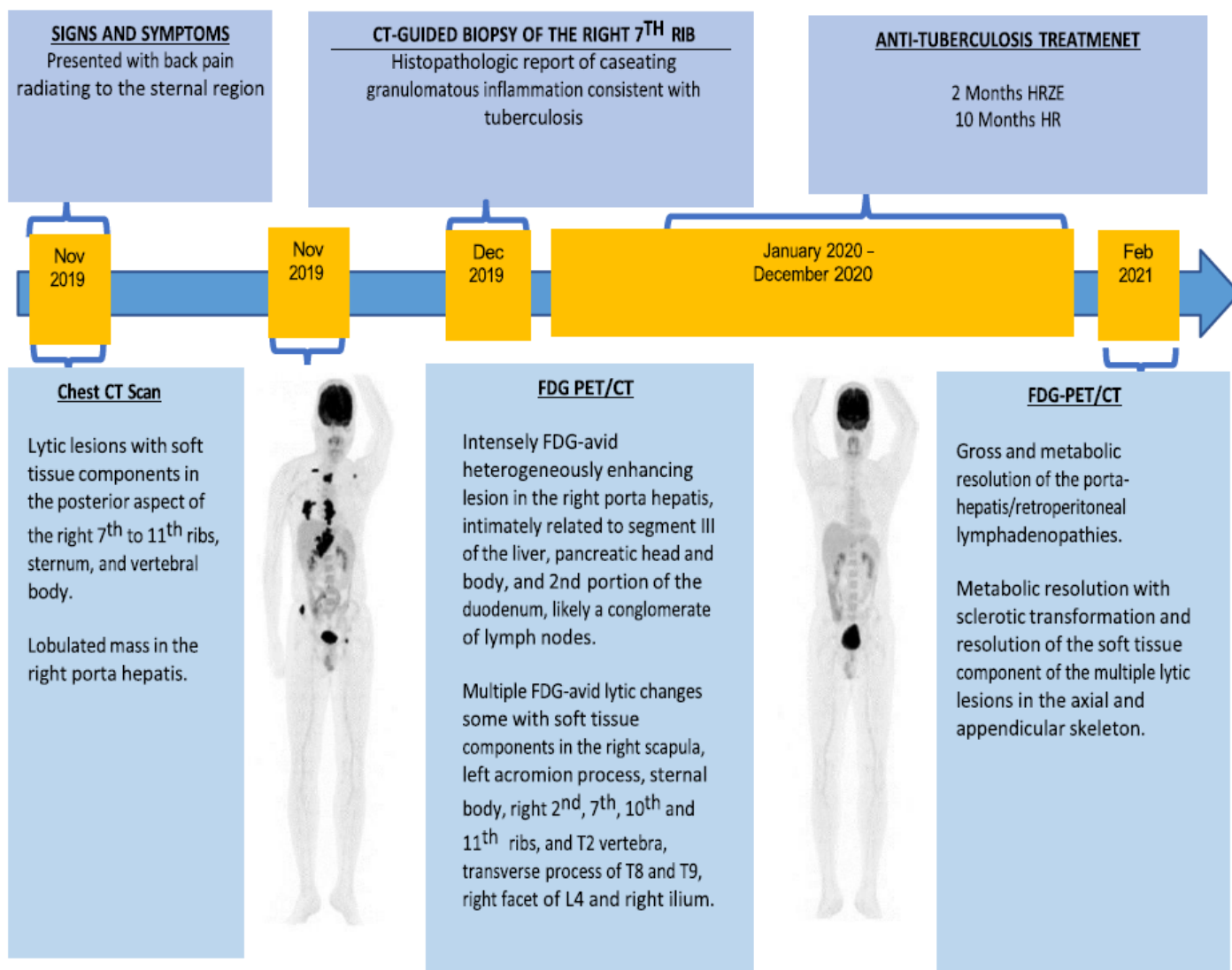
## Diagnostic, Treatment, and Outcome

A chest CT scan revealed lytic lesions with soft tissue components in the posterior aspect of the right 7th to

11th ribs, sternum, and vertebral body, along with a lobulated mass adjacent to the porta hepatis, closely associated with liver segment III and the pancreatic neck. These findings raised suspicion of malignancy, prompting a referral for whole-body FDG PET/CT evaluation.

The PET/CT scan demonstrated intense FDG uptake in the lobulated mass near the porta hepatis, extending to liver segment III, the pancreatic head and body, and the second portion of the duodenum, measuring  $6.2 \times 5.5 \times 4.8$  cm. This was suggestive of a conglomerate of enlarged lymph nodes, with a maximal SUV (SUVmax) of 30. Additionally, multiple FDG-avid (SUVmax up to 39) lytic lesions, some with soft tissue components, were identified in the right scapula, left acromion, sternal body, right 2nd, 7th, 10th, and 11th ribs, T2 vertebra, transverse processes of T8 and T9, right L4 facet, and right ilium.

### TIMELINE



These findings suggested a malignant process, with primary considerations of lymphoma, plasmacytoma, and metastatic disease. To confirm the diagnosis, a CT-guided biopsy of the right 7th rib lesion was performed, revealing caseating granulomatous inflammation consistent with tuberculosis. Further testing, including an acid-fast stain of the sputum, was negative. After a thorough evaluation, a final diagnosis of extrapulmonary tuberculosis (EPTB) was made, affecting the porta hepatis/retroperitoneal lymph nodes and multiple osseous sites.

The patient was treated with a 12-month anti-TB regimen, consisting of two months of isoniazid (H), rifampicin (R), pyrazinamide (Z), and ethambutol (E), followed by 10 months of isoniazid and rifampicin (HR).

After therapy, a follow-up FDG PET/CT scan showed resolution of the abdominal lymphadenopathies and sclerotic transformation of the osseous lesions, suggestive of a favorable treatment response with the anti-TB regimen (Figure 1).

## Discussion

Tuberculosis is a common disease in the Philippines, and nearly 70 Filipinos die every day because of it. According to the world health organization (WHO) global report in 2020, the Philippines has the highest TB incidence rate in Asia [1-2].

General symptoms of TB include weakness, weight loss, fever, and night sweats, but for patients with pulmonary TB, additional symptoms of coughing, chest pain, and hemoptysis may be evident. EPTB manifestations vary, with musculoskeletal involvement leading to back pain, kyphotic deformity of the spine, limb weakness, and paraplegia, whereas lymphatic TB often presents with non-tender palpable nodes [3-7]. In this case, the patient presented with isolated back pain radiating to the sternum without the characteristic symptoms of TB. Given his presentation, a chest CT scan was warranted, which revealed lytic lesions with soft tissue components in the ribs, vertebrae, and sternum, likely contributing to

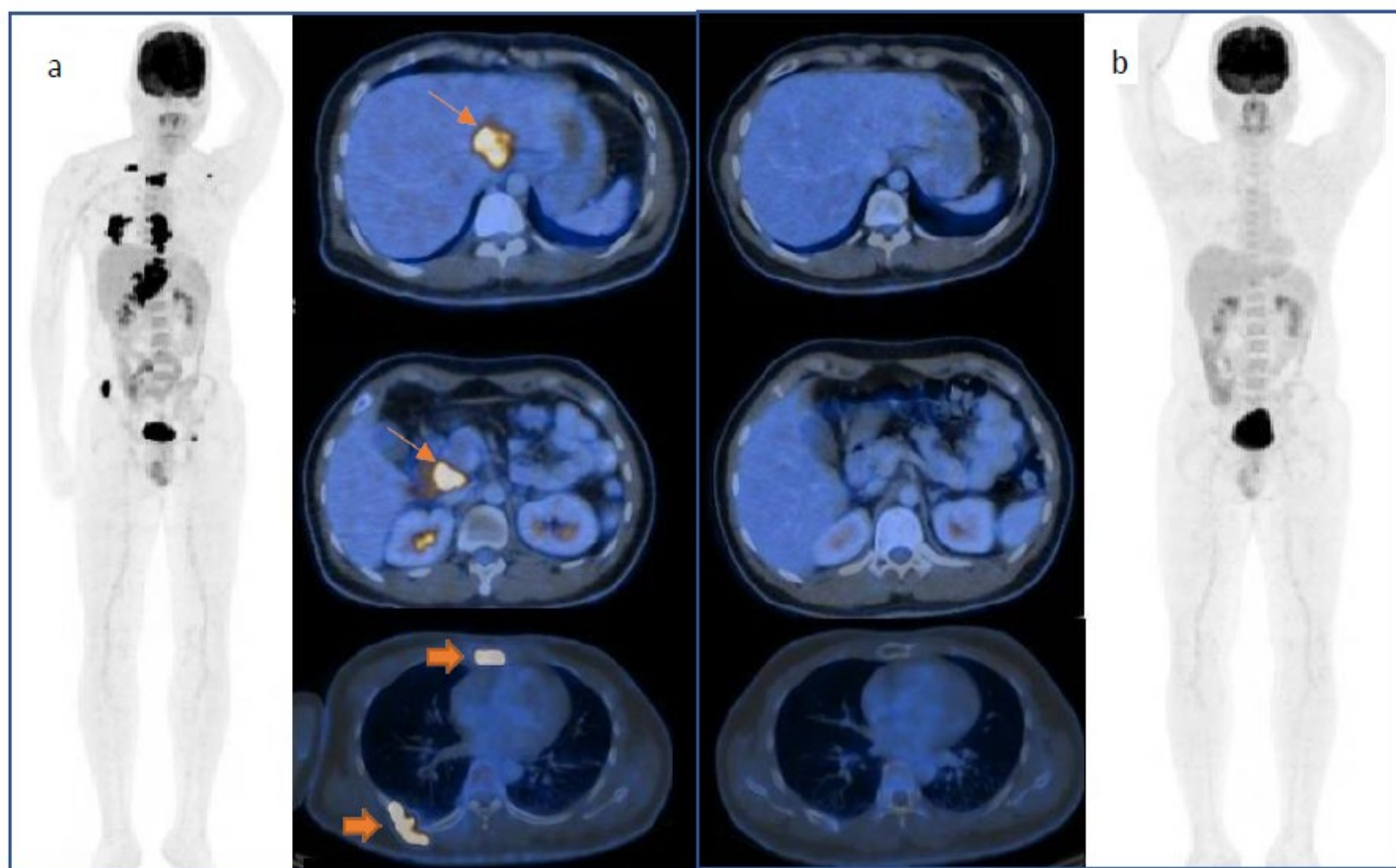


**Figure 1** a) Maximum intensity projection (MIP) and axial cut of the initial FDG PET/CT scan of the patient exhibiting an FDG-avid lobulated mass (↘) in the peri-hepatic region, adjacent to segment III of the liver, pancreatic head, and in the second portion of the duodenum, likely representing a conglomerate of lymph nodes. FDG-avid lytic lesions (→) with soft tissue components in the right sternum and 7th posterior rib. b) MIP and axial cut of the post-therapy FDG PET/CT scan of the case showing metabolic resolution of the lobulated mass, and metabolic resolution with the sclerotic transformation of the osseous lesions.

the patient's pain. A lobulated mass was also identified in the periportal region, raising suspicion for a malignant process. The diagnosis of EPTB is often difficult due to its variable clinical presentations, which can overlap with malignancies, as observed in this case. Hence, an FDG PET/CT scan was done for further evaluation.

FDG-PET/CT enables molecular imaging of physiological and biochemical processes and is extensively utilized in oncologic assessment. FDG uptake corresponds to elevated glycolytic activity in malignant tumors, yet it is not tumor-specific, as it can also accumulate in infectious and inflammatory conditions. Lesion metabolic activity is quantified using the standardized uptake value (SUV), with values exceeding 2.5 generally considered suspicious for malignancy. However, infectious and inflammatory processes, including TB, may demonstrate comparably increased SUV levels, posing a diagnostic dilemma [8-9].

The increased uptake of FDG in tumor cells is primarily driven by the upregulation of glucose transporters (GLUT) and elevated intracellular levels of hexokinase and phosphofructokinase, key enzymes that enhance glycolytic activity. Malignant cells exhibit a heightened glycolytic rate, a phenomenon known as the Warburg effect, leading to the intracellular accumulation of FDG, a glucose analog that undergoes phosphorylation to 2-[18F] fluoro-2-deoxyglucose-6-phosphate (FDG-6-phosphate) and remains trapped within the cell [8-10]. Similarly, activated inflammatory cells, including macrophages, monocytes, neutrophils, and lymphocytes, demonstrate increased glucose metabolism, contributing to FDG accumulation in sites of infection and inflammation [11-12]. TB, as an infectious process, induces a strong inflammatory response, leading to FDG uptake patterns that overlap with those of malignancies, thereby complicating differentiation between active TB and cancer on FDG PET/CT imaging [11-12].

Recent studies have demonstrated FDG accumulation in immune cells involved in various stages of TB infection. Following infection with *M. tuberculosis*, macrophages undergo M1 polarization, a process associated with metabolic reprogramming that enhances glycolytic flux. This metabolic shift leads to the upregulation of GLUT and hexokinase, key regulators of FDG uptake [12-18]. Early macrophage activation is critical for the production of antimicrobial and pro-inflammatory mediators, facilitating granuloma formation to contain the infection and prevent its dissemination [12-18]. Granulomas, composed of macrophages, lymphocytes, neutrophils, and fibroblasts, also exhibit increased FDG uptake

[12-18]. Multiple studies have reported FDG PET/CT positivity in patients histopathologically diagnosed with TB, reinforcing that FDG is not a tumor-specific tracer and may lead to false-positive findings, particularly in individuals with active infections such as TB [12-18].

The definitive diagnosis of EPTB requires biopsy and histopathological examination of the affected organ [19]. Once confirmed, a standard anti-TB regimen is initiated, typically consisting of a six- to nine-month course: an initial two-month phase with isoniazid (H), rifampicin (R), pyrazinamide (Z), and ethambutol (E), followed by a continuation phase of four to seven months with isoniazid and rifampicin [19-21]. In cases involving bone and joint TB, prolonged therapy may be necessary. In this case, a 12-month regimen (2HRZE/10HR) was administered.

Post-treatment FDG PET/CT, in this case, showed resolution of abdominal lymphadenopathy, the sclerotic transformation of bone lesions, and the disappearance of soft tissue components, indicating a positive treatment response. Evidence suggests that FDG PET/CT plays a valuable role in assessing treatment response in EPTB, particularly in complex cases [14].

## Conclusion

Tuberculosis is one of the most prevalent infectious diseases, with diverse presentations that can involve various organs of the body. Distinguishing EPTB with subtle symptoms from malignancy is challenging, making diagnosis difficult. EPTB can exhibit elevated FDG uptake in PET/CT scans, potentially leading to false-positive results. Therefore, in patients presenting with lymphadenopathies and bone lesions, increased FDG avidity on PET/CT scans does not always indicate malignant disease, and EPTB should be considered, particularly in individuals from endemic regions such as the Philippines. Pathological examination remains crucial for accurately diagnosing EPTB.

## Consent

Informed consent was obtained from the patient. This case report follows the protection and confidentiality of the patient in accordance with the Data Privacy Act of 2012 and in the rules and principles of the 1964 Declaration of Helsinki.

## REFERENCES

- World Health Organization. Global tuberculosis report 2020. <https://www.who.int/publications/item/9789240013131>.
- Sia, I. G., & Wieland, M. L. (2011). Current concepts in the management of tuberculosis. *Mayo Clinic proceedings*, 86(4), 348–361. <https://doi.org/10.4065/mcp.2010.0820>
- Peto, H. M., Pratt, R. H., Harrington, T. A., LoBue, P. A., & Armstrong, L. R. (2009). Epidemiology of extrapulmonary tuberculosis in the United States, 1993–2006. *Clinical infectious diseases : an official publication of the Infectious Diseases Society of America*, 49(9), 1350–1357. <https://doi.org/10.1086/605559>
- Harkirat, S., Anana, S., Indrajit, L., & Dash, A. (2008). Pictorial essay: PET/CT in tuberculosis. *The Indian Journal of Radiology & Imaging*, 18(2), 141–147.
- Dandapat, M. C., Mishra, B. M., Dash, S. P., & Kar, P. K. (1990). Peripheral lymph node tuberculosis: a review of 80 cases. *The British journal of surgery*, 77(8), 911–912. <https://doi.org/10.1002/bjs.1800770823>.
- Garg, R. K., & Somvanshi, D. S. (2011). Spinal tuberculosis: a review. *The journal of spinal cord medicine*, 34(5), 440–454. <https://doi.org/10.1179/2045772311Y.0000000023>.
- Boellaard, R., Delgado-Bolton, R., Oyen, W. J., Giammarile, F., Tatsch, K., Eschner, W., Verzijlbergen, F. J., Barrington, S. F., Pike, L. C., Weber, W. A., Stroobants, S., Delbeke, D., Donohoe, K. J., Holbrook, S., Graham, M. M., Testanera, G., Hoekstra, O. S., Zijlstra, J., Visser, E., Hoekstra, C. J., ... European Association of Nuclear Medicine (EANM) (2015). FDG PET/CT: EANM procedure guidelines for tumour imaging: version 2.0. *European journal of nuclear medicine and molecular imaging*, 42(2), 328–354. <https://doi.org/10.1007/s00259-014-2961-x>.
- Chang, J. M., Lee, H. J., Goo, J. M., Lee, H. Y., Lee, J. J., Chung, J. K., & Im, J. G. (2006). False positive and false negative FDG-PET scans in various thoracic diseases. *Korean journal of radiology*, 7(1), 57–69. <https://doi.org/10.3348/kjr.2006.7.1.57>
- Metser, U., & Even-Sapir, E. (2007). Increased (18)F-fluorodeoxyglucose uptake in benign, nonphysiologic lesions found on whole-body positron emission tomography/computed tomography (PET/CT): accumulated data from four years of experience with PET/CT. *Seminars in nuclear medicine*, 37(3), 206–222. <https://doi.org/10.1053/j.semnuclmed.2007.01.001>.
- Hahm, C. R., Park, H. Y., Jeon, K., Um, S. W., Suh, G. Y., Chung, M. P., Kim, H., Kwon, O. J., & Koh, W. J. (2010). Solitary pulmonary nodules caused by *Mycobacterium tuberculosis* and *Mycobacterium avium* complex. *Lung*, 188(1), 25–31. <https://doi.org/10.1007/s00408-009-9203-1>.
- Kim, I. J., Lee, J. S., Kim, S. J., Kim, Y. K., Jeong, Y. J., Jun, S., Nam, H. Y., & Kim, J. S. (2008). Double-phase 18F-FDG PET-CT for determination of pulmonary tuberculoma activity. *European journal of nuclear medicine and molecular imaging*, 35(4), 808–814. <https://doi.org/10.1007/s00259-007-0585-0>.
- Priftakis, Dimitris & Riaz, Saima & Zumla, Alimuddin & Bomanji, Jamshed. (2020). Towards more accurate 18F-fluorodeoxyglucose positron emission tomography (18F-FDG PET) imaging in Active and Latent Tuberculosis. *International journal of infectious diseases : IJID : official publication of the International Society for Infectious Diseases*, 92S, S85–S90. <https://doi.org/10.1016/j.ijid.2020.02.017>.
- Shi, L., Jiang, Q., Bushkin, Y., Subbian, S., & Tyagi, S. (2019). Biphasic Dynamics of Macrophage Immunometabolism during *Mycobacterium tuberculosis* Infection. *mBio*, 10(2), e02550-18. <https://doi.org/10.1128/mBio.02550-18>.
- Yamada, S., Kubota, K., Kubota, R., Ido, T., & Tamahashi, N. (1995). High accumulation of fluorine-18-fluorodeoxyglucose in turpentine-induced inflammatory tissue. *Journal of nuclear medicine : official publication, Society of Nuclear Medicine*, 36(7), 1301–1306.
- Yago, Y., Yukihiro, M., Kuroki, H., Katsuragawa, Y., & Kubota, K. (2005). Cold tuberculous abscess identified by FDG PET. *Annals of nuclear medicine*, 19(6), 515–518. <https://doi.org/10.1007/BF02985581>.
- Chen, Y. K., Shen, Y. Y., & Kao, C. H. (2004). Abnormal FDG PET imaging in tuberculosis appearing like lymphoma. *Clinical nuclear medicine*, 29(2), 124. <https://doi.org/10.1097/01.rlu.0000109300.89514.35>.
- Yang, C. M., Hsu, C. H., Lee, C. M., & Wang, F. C. (2003). Intense uptake of [F-18]-fluoro-2 deoxy-D-glucose in active pulmonary tuberculosis. *Annals of nuclear medicine*, 17(5), 407–410. <https://doi.org/10.1007/BF03006610>.
- Heysell, S. K., Thomas, T. A., Sifri, C. D., Rehm, P. K., & Houpt, E. R. (2013). 18-Fluorodeoxyglucose positron emission tomography for tuberculosis diagnosis and management: a case series. *BMC pulmonary medicine*, 13, 14. <https://doi.org/10.1186/1471-2466-13-14>.
- Borchert, T., Beitar, L., Langer, L. B. N., Polyak, A., Wester, H. J., Ross, T. L., Hilfiker-Kleiner, D., Bengel, F. M., & Thackeray, J. T. (2021). Dissecting the target leukocyte subpopulations of clinically relevant inflammation radiopharmaceuticals. *Journal of nuclear cardiology : official publication of the American Society of Nuclear Cardiology*, 28(4), 1636–1645. <https://doi.org/10.1007/s12350-019-01929-z>
- Lee J. Y. (2015). Diagnosis and treatment of extrapulmonary tuberculosis. *Tuberculosis and respiratory diseases*, 78(2), 47–55. <https://doi.org/10.4046/trd.2015.78.2.47>.

21. Implementing the WHO Stop TB Strategy: A Handbook for National Tuberculosis Control Programmes. Geneva: World Health Organization; 2008. 2, Treatment of tuberculosis patients.
22. Ankrah, A. O., van der Werf, T. S., de Vries, E. F., Dierckx, R. A., Sathekge, M. M., & Glaudemans, A. W. (2016). PET/CT imaging of Mycobacterium tuberculosis infection. Clinical and translational imaging, 4, 131–144. <https://doi.org/10.1007/s40336-016-0164-0>.

# Evaluation of Bone Graft Viability Using Three-Phase Bone Scan with Single Photon Emission Tomography (SPECT): A Case Series

Louen Mark T. Visaya, MD

Department of Nuclear Medicine, Jose R. Reyes Memorial Medical Center

E-mail address: louenmarkvisaya@gmail.com

## ABSTRACT

*Autologous bone grafts are fundamental in orthopedic procedures, and ensuring graft viability is pivotal. Three-phase bone scans with single photon emission computed tomography (SPECT) show promise for assessing graft health. This case series evaluates the potential of three-phase bone scans with SPECT for predicting graft viability and postoperative monitoring. Two cases were studied, representing different age groups, both undergoing orthopedic procedures with bone grafts. One case initially exhibited signs of poor graft viability but showed subsequent clinical improvement. The other case demonstrated robust graft viability, mirroring positive clinical progress.*

*This study underscores the potential of three-phase bone scans with SPECT for graft viability assessment. Larger studies are warranted to validate these findings across diverse patient profiles and clinical scenarios.*

## INTRODUCTION

Autologous bone graft is widely recognized as the gold standard for bone grafting in various medical and surgical contexts, owing to its superior efficacy compared to allografts [1]. The use of autologous bone grafts offers several advantages, including reduced risk of graft rejection and the potential for enhanced healing and integration [2]. One of the most common sources of autologous bone grafts is the iliac spine, a region that provides ample graft material while minimizing donor site morbidity. [3] Despite its effectiveness, the success of autologous bone grafts is contingent upon various factors, and the ability to predict and ensure graft viability is of paramount importance in achieving positive patient outcomes.

The effectiveness of three-phase bone scans in predicting bone graft viability has been highlighted in several prior studies [1][4]. This scan is a non-invasive imaging modality that can provide valuable insights into the perfusion and metabolic activity of the graft site. By assessing blood flow, perfusion, and bone turnover, three-phase bone scans offer a dynamic and comprehensive evaluation of graft viability. This has the

potential to serve as an early warning system for graft complications, allowing clinicians to take proactive measures to address any issues before they result in graft failure.

## OBJECTIVES

This case series aims to contribute to the growing body of knowledge surrounding the use of three-phase bone scans in bone grafting procedures. By evaluating their utility in predicting the viability of autologous bone grafts, the researcher seeks to provide clinicians with a potentially valuable tool for enhancing the success of these critical procedures. Through the examination of real-life cases and the analysis of three-phase bone scan data, we aim to offer insights that can inform clinical practice, reduce graft-related complications, and ultimately improve patient outcomes.

### Inclusion Criteria

This study included patients who underwent an orthopedic procedure involving bone grafting and subsequently underwent three-phase bone scans to assess graft viability.

## Case 1

The patient is N.A., a 71-year-old female with history of vehicular accident 1 month prior to scan resulting in the fracture of her left thigh. Patient sought consult at JRRMMC where she was assessed as a case of closed, complete, displaced, comminuted fracture of the left distal femur. Patient was advised surgery and underwent Open Reduction with Internal Fixation using Plate and Screws with Iliac Crest Bone Graft of the Left Distal Femur 7 days prior to scan. A three-phase bone scan was requested 7 days post-operatively to assess graft viability (Fig 2.1-2.3).

On the day of the scan, the patient was noted to be in good pain control (PS 3/10) but is not able to ambulate due to exacerbation of pain upon movement. Perfusion phase images (Figure 1.1A) show that there is symmetrical blood flow/supply to the bilateral thighs while the soft tissue phase images (Figure 1.1B) show an area of decreased radiotracer in the region of the distal

3rd of the left thigh. In contrast, the right thigh exhibits homogenous soft tissue radiotracer distribution .

Delayed imaging (Figure 1.2) 2 hours after radiotracer administration showed washout of soft tissue activity. There is an area of decreased radiotracer uptake appreciated on the distal 3rd of the left femur coinciding with the site of the bone graft with increased radiotracer localization around the photopenic area. Single Photon Emission Tomography (SPECT) (Figure 1.3) was done showing an area of decreased radiotracer uptake on the site of the bone graft. These findings were interpreted as suggestive of poor bone graft viability.

In the interim, the patient was reported to have an improving clinical picture. The patient was noted to be able to ambulate with assistance and pain medications were reported to be necessary on an as needed basis only. A follow-up three-phase bone scan (Fig 2.1-2.3) was requested 6 weeks after the first scan

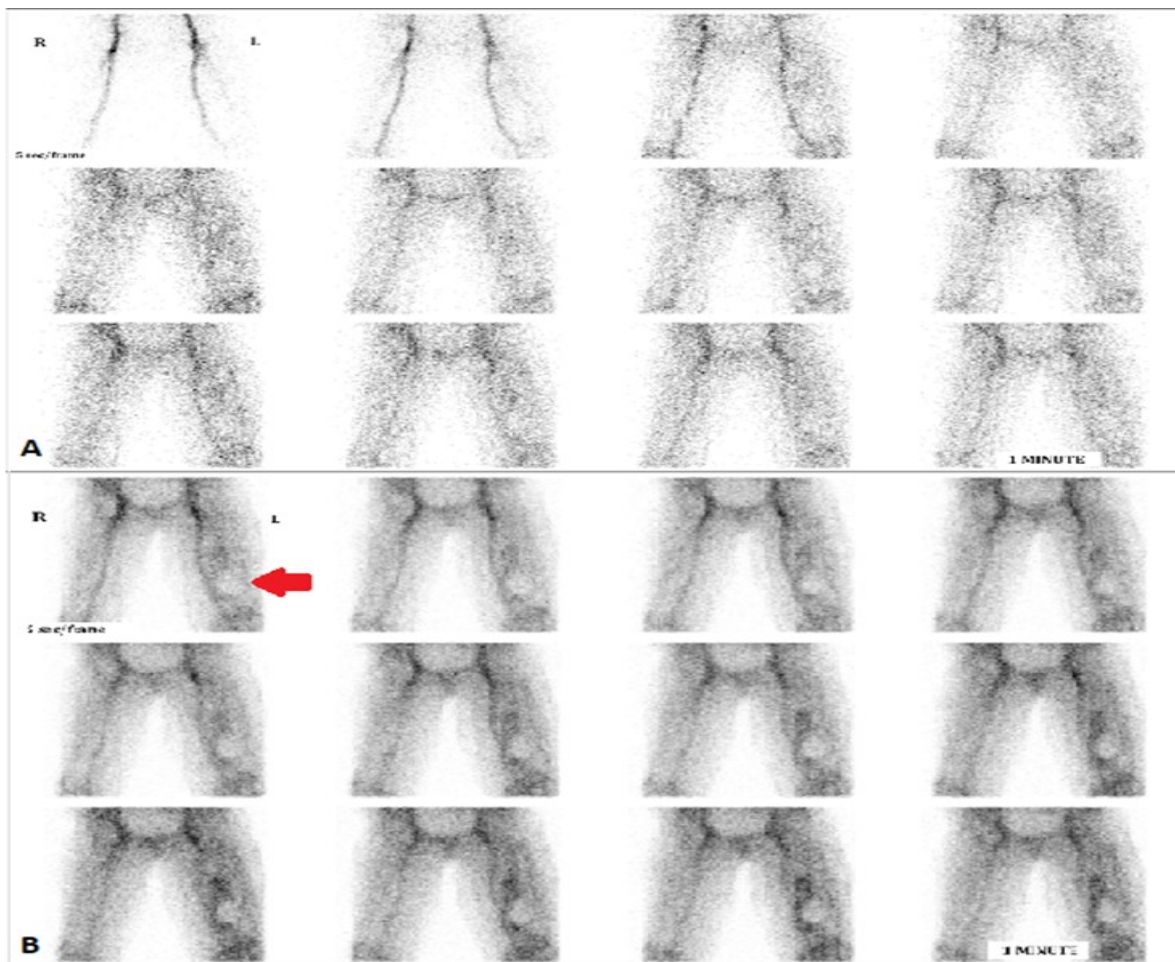


**FIGURE 1.1** Perfusion and flow phase images in anterior projection using Tc-99m HDP: (A) Perfusion phase images show symmetrical blood flow in the bilateral thighs; (B) Flow phase images show a photopenic defect (red arrow) in the region of the distal 3rd of the left thigh.

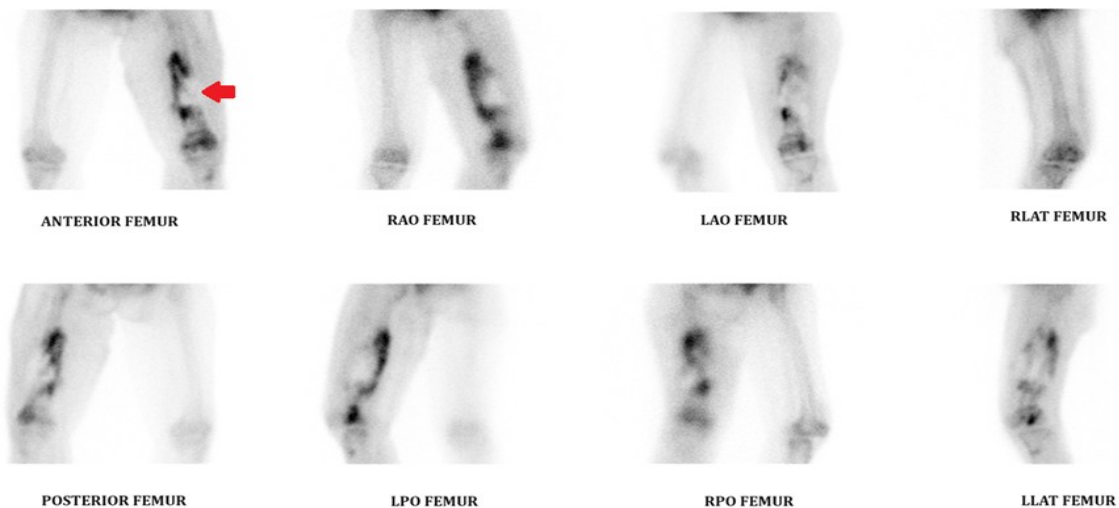


**FIGURE 1.2** Delayed images in multiple views with persistence of photopenic defect at the graft site (red arrow).



**FIGURE 1.3** Single Photon Emission Tomography (SPECT) images of the left femur still show a photopenic area at the graft site

Perfusion phase images (Figure 2.1A) show that there is symmetrical blood flow/supply to the bilateral thighs while the soft tissue phase images (Figure 2.1B) show homogenous and symmetrical radiotracer distribution. The previously noted area of decreased radiotracer uptake in the region of the distal 3rd of the left thigh is no longer appreciated.

Delayed imaging (Figure 2.2) 2 hours after radiotracer

administration showed washout of soft tissue activity. There is still an area of decreased but comparatively improved radiotracer uptake appreciated on the distal 3rd of the left femur coinciding with the site of the bone graft. Single Photon Emission Tomography (SPECT) (Figure 2.3) likewise showed an area of decreased but comparatively improved radiotracer uptake radiotracer uptake on the site of the bone graft.

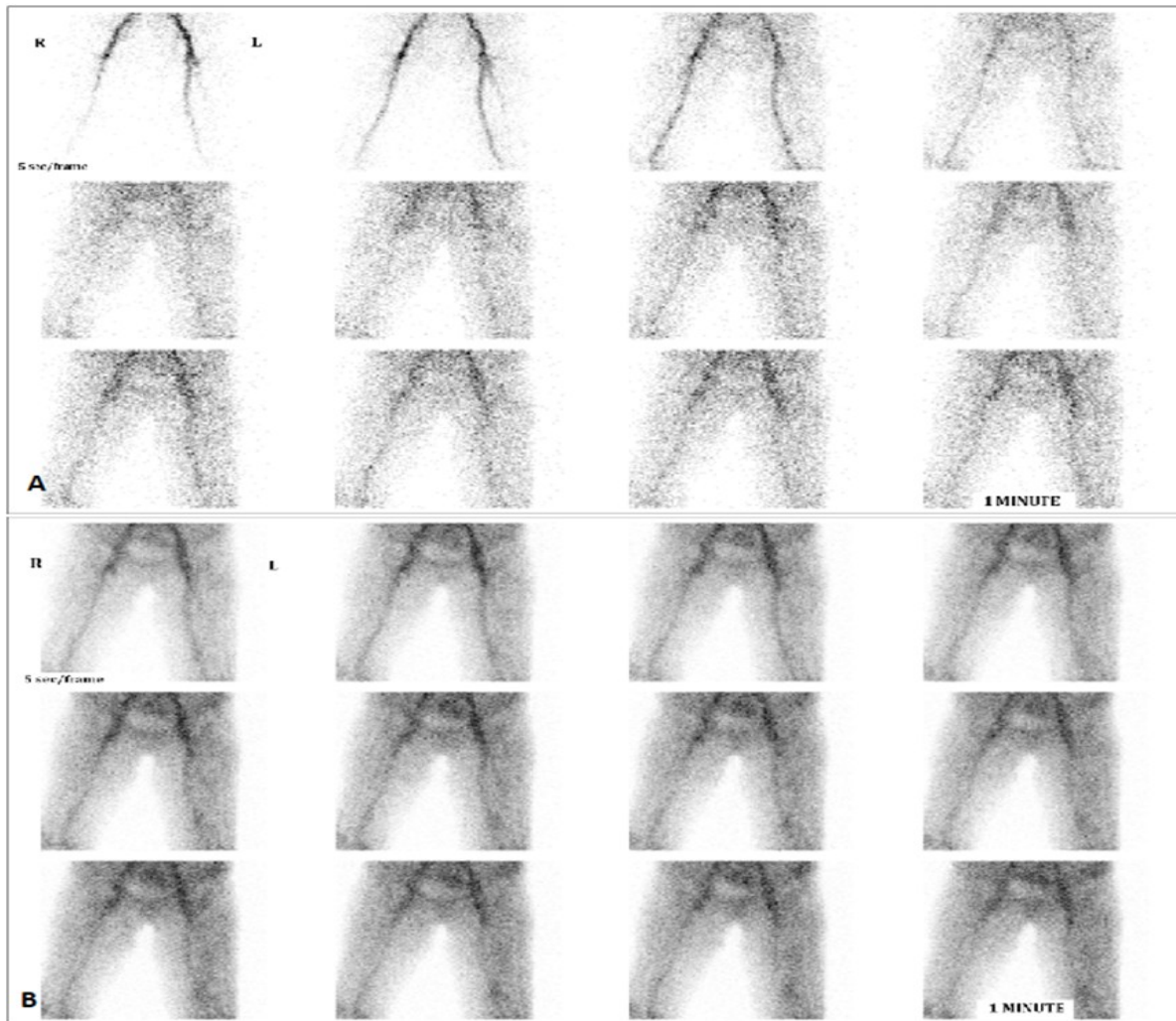


**FIGURE 2.1** Perfusion and flow phase images in anterior projection using Tc-99m HDP: (A) Perfusion phase images show symmetrical and normal blood flow in the bilateral thighs; (B) Flow phase images show homogenous radiotracer uptake on both thighs.

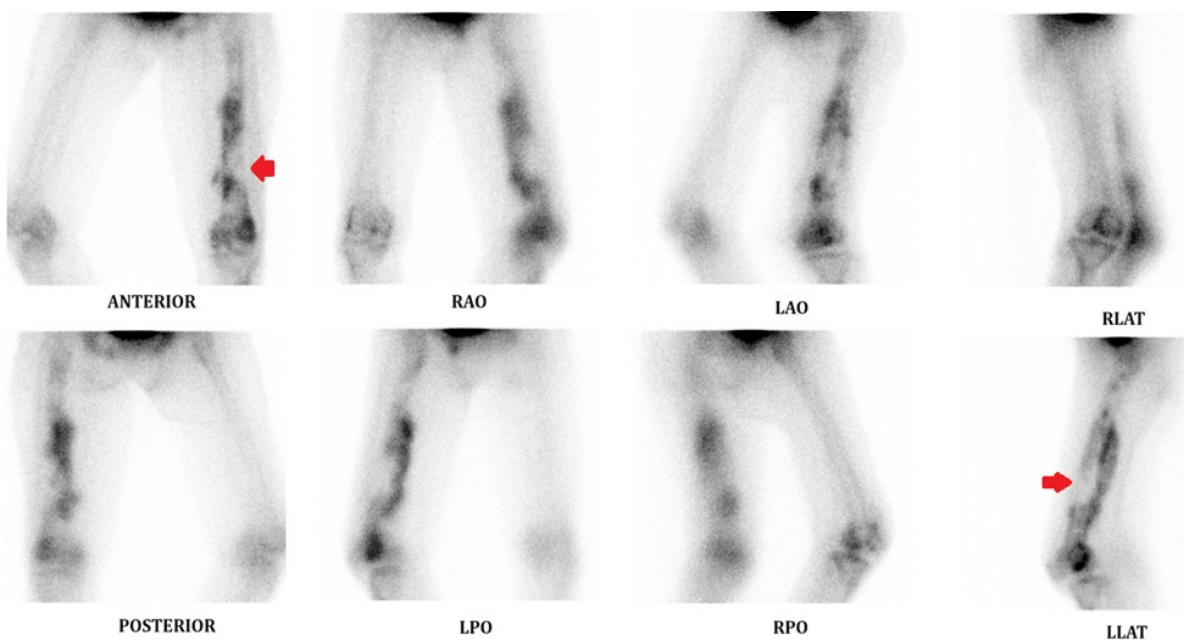


**FIGURE 2.2** Delayed images in multiple views show faint radiotracer localization at the graft site (red arrow).

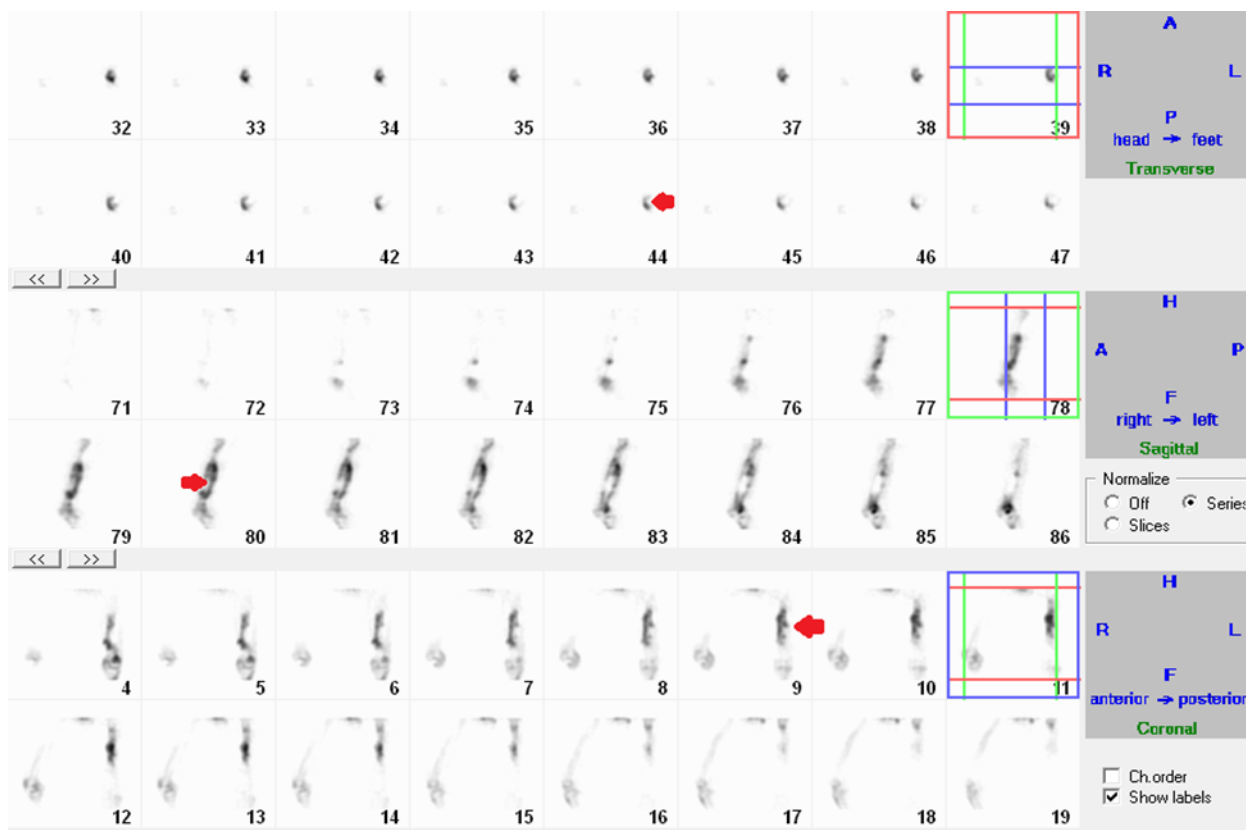


**FIGURE 2.3** Single Photon Emission Tomography (SPECT) images of the left femur still show faint localization of radiotracer at the graft site.

## Case 2

The patient is G.D.L., a 13-year-old male with a known history of congenital pseudoarthrosis of the left distal tibia secondary to neurofibromatosis. The patient underwent resection of neurofibroma at the left distal tibia with application of Ilizarov external fixator 9 years prior to the scan. In the interim there was noted lag in the growth of the left leg compared to the right leg with development of pseudoarthrosis hence consult at our institution where he was advised to undergo operation. Eight days prior to the scan, patient underwent resection of the pseudoarthrosis with iliac crest bone graft and application of Ilizarov external applicator. A three-phase bone scan was requested 7 days post-operatively to assess graft viability.

On the day of the scan, the patient was noted to be in good pain control (PS 4/10) but is not able to ambulate due to exacerbation of pain and the presence of the Ilizarov fixator. Perfusion phase images (Figure 3.1A) show that there is an area of increased blood flow along the region of the distal half of the left leg in comparison with the contralateral leg. Soft tissue phase images

(Figure 3.1B) show an area of increased radiotracer distribution on the distal leg. In contrast, the right leg exhibits homogenous soft tissue radiotracer distribution.

Delayed imaging (Figure 3.2) 2 hours after radiotracer administration showed washout of soft tissue activity with increased radiotracer uptake appreciated on the distal 3rd of the left tibia coinciding with the site of the bone graft. SPECT imaging (Figure 3.3) was done showing an area of increased radiotracer uptake on the site of the bone graft. These findings were interpreted as indicative of good bone graft viability.

## DISCUSSION

Three-phase bone scan with SPECT can offer a unique perspective on the physiological activity of bone grafts. Unlike structural imaging techniques, scintigraphy is characterized by its capacity to provide insight into the metabolic activity of the bone, making it particularly well - suited for the assessment of graft integrity and viability [1][4][5][6]. The three-phase component of the bone scan can potentially serve a pivotal role in our assessment of graft viability, as it primarily indicates

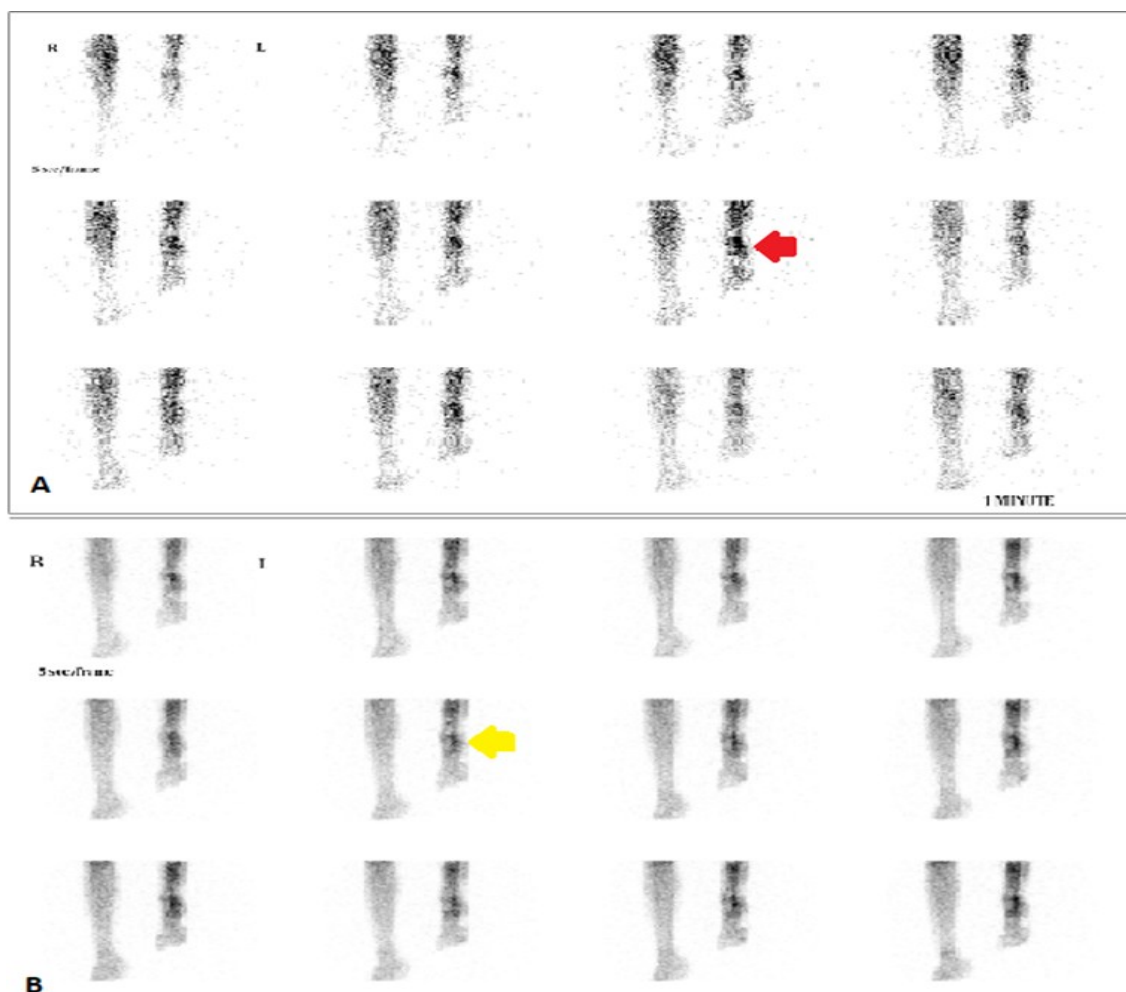


**FIGURE 3.1** Perfusion and flow phase images in anterior projection using Tc-99m HDP: (A) Perfusion phase images show increased blood flow (red arrow) at the distal half of the left leg; (B) Flow phase images show increased radiotracer accumulation (yellow arrow) at the site of the bone graft .

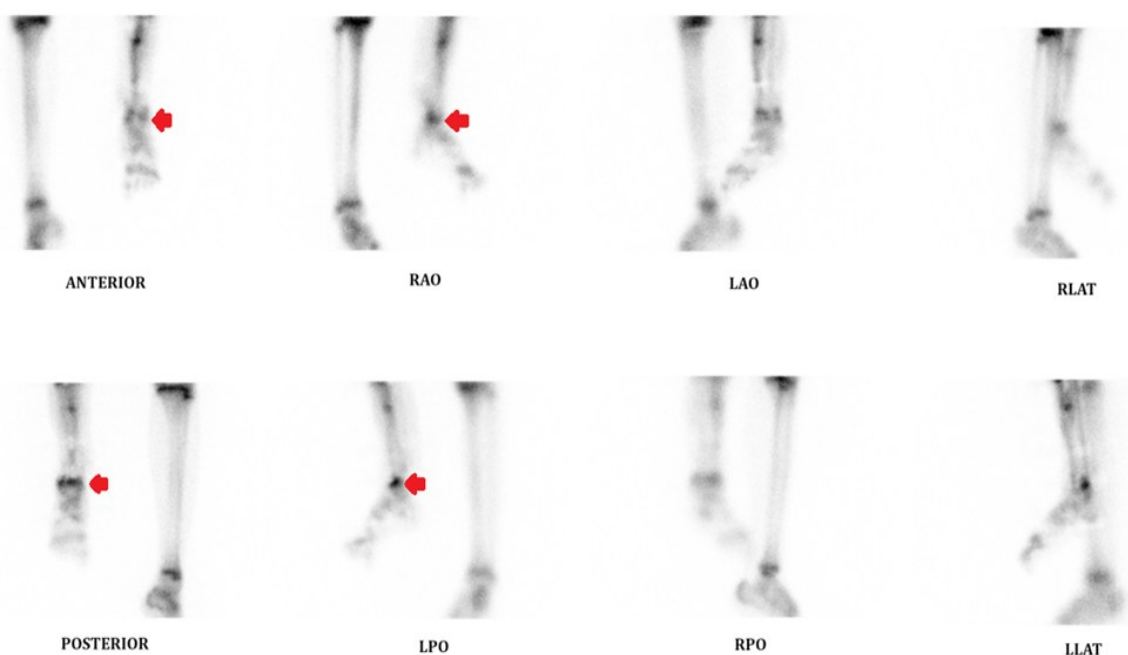


**FIGURE 3.2** Delayed images in multiple views with increased radiotracer uptake at the graft site (red arrows).

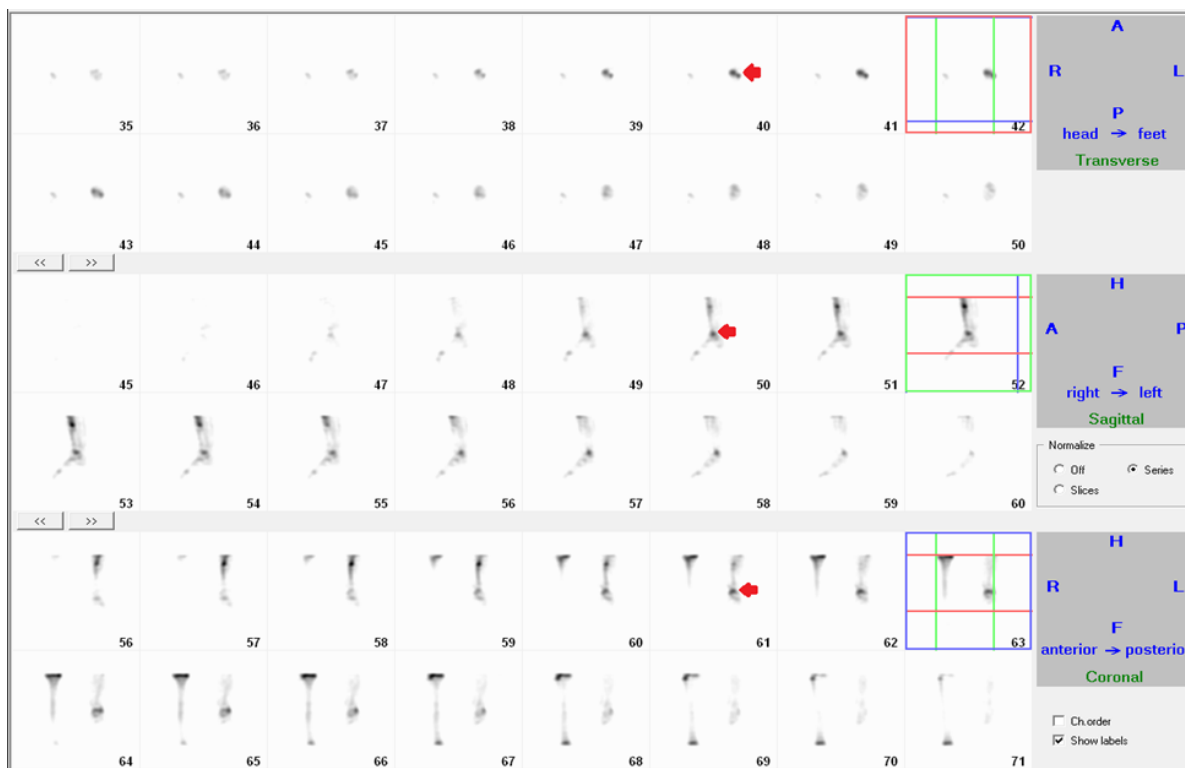


**FIGURE 3.3** Single Photon Emission Tomography (SPECT) images show increased radiotracer uptake at the graft site.

blood flow within the graft region. Elevated tracer uptake during the early phase of the scan signifies the preservation of blood supply to the graft region, highlighting the critical role of vascularization in graft viability. Furthermore, the images obtained at later stages of the scan reveal increased tracer uptake, corroborating the integrity and viability of the bone graft.

At one week post-operation, Case 1 showed a notable decrease in graft area uptake across all three phases of the scan, whereas Case 2 displayed an increased uptake in the graft area in all three phases. In the context of our investigation, a 'triple positive' scan, obtained one week after surgery, typically indicates robust graft viability and predicts favorable outcomes [7]. Conversely, a 'triple negative' scan is often associated with poor graft viability and potential complications [7]. Initially, our observations led us to anticipate potential graft viability challenges and clinical outcome uncertainties for Case 1, while Case 2 appeared to be on track for a positive clinical course. However, the clinical team decided to closely monitor Case 1 for any signs of improvement. Remarkably, over the following period, the patient demonstrated clinical progress. What's particularly noteworthy is that our findings align with existing research, which suggests that even in cases where early postoperative scans indicate suboptimal graft viability, subsequent follow-up assessments can reveal

improvement [8]. This improvement is often evident in both the imaging data and the patient's clinical presentation. These observations highlight the potential value of postoperative follow-up scans in the ongoing monitoring and management of graft outcomes, offering crucial insights, especially in cases where initial scans might raise concerns about graft viability.

Case 1 presents an intriguing aspect of this study. As an elderly patient, N.A. was subjected to the rigors of a major orthopedic procedure. It is important to consider that advanced age can introduce certain factors that may affect the graft's healing process, potentially leading to a more delayed response [9]. This delay could explain the initial 'triple negative' scan, suggesting poor graft viability. The subsequent improvement observed in Case 1 underscores the possibility of delayed healing and the importance of patience in the evaluation of graft viability, especially in older individuals. These findings highlight the need for a tailored approach in assessing graft outcomes, accounting for patient-specific factors such as age.

It is also vital to recognize that the insights gained from this study may not universally apply to all patients and graft scenarios. The cases presented here offer valuable glimpses into the potential of three-phase bone scans with SPECT as a predictive tool for graft viability.

However, the sample size is limited, and variations in patient demographics, surgical techniques, and graft sites can influence outcomes. Therefore, it is crucial to exercise caution when generalizing these findings to a broader population. Larger case series or multicenter studies are warranted to establish a more comprehensive consensus regarding the utility of this diagnostic modality in predicting bone graft viability across diverse patient profiles and clinical settings.

## CONCLUSION

In conclusion, this case series has shed light on the potential of three-phase bone scans with SPECT as a valuable tool in assessing the viability of bone grafts in orthopedic procedures. The findings underscore the dynamic nature of graft viability and the importance of considering individual patient characteristics, including age, in the assessment of graft outcomes. The cases of an elderly patient (Case 1) and a young patient (Case 2) demonstrated the varying responses to grafts and highlighted the need for patience and careful monitoring in the evaluation of graft viability, especially in older individuals.

Furthermore, the study highlights the significance of sequential scans in tracking the progression of graft viability over time. The initial 'triple negative' scan observed in Case 1 raised concerns about graft viability, but subsequent follow-up scans revealed improvement, aligning with the patient's clinical progress. This emphasizes the potential value of postoperative follow-up scans as an essential component of graft outcome management.


However, it is essential to acknowledge the limitations of this study. The sample size is limited, and the insights gained may not universally apply to all patient populations and graft scenarios. The results presented here serve as a foundation for further research in this field, encouraging larger case series and multicenter studies to establish a more comprehensive consensus on the utility of three-phase bone scans with SPECT in predicting bone graft viability. Such endeavors will contribute to the refinement of clinical practice and the enhancement of patient outcomes in orthopedic surgery.

## REFERENCES

1. Hashim, M. H., Ali, S., Usman, N., Hashim, M. N., Malik, M. A., Zahid, S., & Akhter, M. U. (2019). Assessment of Bone Graft Viability Using Scintigraphy. *Oral and Maxillofacial*

*Surgery*, 39(3), 230-33.

2. Egol, K. A., Nauth, A., Lee, M., Pape, H. C., Watson, J. T., & Borrelli, J., Jr (2015). Bone Grafting: Sourcing, Timing, Strategies, and Alternatives. *Journal of orthopaedic trauma*, 29 Suppl 12, S10–S14. <https://doi.org/10.1097/BOT.0000000000000460>.
3. Salawu, O. N., Babalola, O. M., Ahmed, B. A., Ibraheem, G. H., & Kadir, D. M. (2017). Comparative Study of Proximal Tibia and Iliac Crest Bone Graft Donor Sites in Treatment of Orthopaedic Pathologies. *Malaysian orthopaedic journal*, 11(2), 15–19. <https://doi.org/10.5704/MOJ.1707.011>.
4. Kim, H., Lee, K., Ha, S., Shin, E., Ahn, K. M., Lee, J. H., & Ryu, J. S. (2020). Predicting Vascularized Bone Graft Viability Using 1-Week Postoperative Bone SPECT/CT After Maxillofacial Reconstructive Surgery. *Nuclear medicine and molecular imaging*, 54(6), 292–298. <https://doi.org/10.1007/s13139-020-00670-7>.
5. Buyukdereli, G., Guney, I. B., Ozerdem, G., & Kesiktas, E. (2006). Evaluation of vascularized graft reconstruction of the mandible with Tc-99m MDP bone scintigraphy. *Annals of nuclear medicine*, 20(2), 89–93. <https://doi.org/10.1007/BF02985619>.
6. Anjali, M., Mohit, D., & Vandana. K. D. (2021). Overview of Imaging Modalities in Evaluation of Bone Allograft Viability . *Journal of Radiation and Nuclear Medicine - 1* (2):1-5. <https://doi.org/10.14302/issn.2766-8630.jrnm-20-3689>.
7. Kim, H., Lee, K., Ha, S., Shin, E., Ahn, K. M., Lee, J. H., & Ryu, J. S. (2020). Predicting Vascularized Bone Graft Viability Using 1-Week Postoperative Bone SPECT/CT After Maxillofacial Reconstructive Surgery. *Nuclear medicine and molecular imaging*, 54(6), 292–298. <https://doi.org/10.1007/s13139-020-00670-7>.
8. Aydogan, F., Akbay, E., Cevik, C., & Kalender, E. (2014). Blood-pool SPECT in addition to bone SPECT in the viability assessment in mandibular reconstruction. *European review for medical and pharmacological sciences*, 18(4), 587–592.
9. Foulke, B. A., Kendal, A. R., Murray, D. W., & Pandit, H. (2016). Fracture healing in the elderly: A review. *Maturitas*, 92, 49–55. <https://doi.org/10.1016/j.maturitas.2016.07.014>.





An established global key  
player in the **radioisotope  
& radiopharmaceutical** field.

Find out more about  
us and our products:



[www.itm-radiopharma.com](http://www.itm-radiopharma.com)

Follow us:  

 **itm**

PASSION FOR PRECISION

*A revolutionary development in radiopharmaceutical production  
that delivers a single or batch dose of [18F]FDG,  
and additional advanced [18F] biomarkers,  
"on demand."*

# ABT B-100 BIOMARKER GENERATOR



*Best* ABT Molecular Imaging

A Healthcare Tech Company

ISO 9001:2015 CERTIFIED

[www.assurancecontrol.com](http://www.assurancecontrol.com)

## RIA Instrument



**Gamma Counter**



**Dispenser**



**Tube Washer**



**Incubator**

**Full Automatic**



## RIA KIT

ITEM	ITEM	ITEM	ITEM
HBsAg(1Step)	T3	Free PSA	B-HCG
Anti-HBs	T4	Ultra PSA	Insulin
Anti-HBc IgG	Free T4	CA125	C-peptide
Anti-HBc IgM	Free T3	CA19-9	Total IgE
Anti-HBc (RIA)	T3-Uptake	AFP	Testosterone
Anti-HAV IgG	TSH	CA15-3	25-Vitamin D total
Anti-HAV IgM	Tg-s	Ferritin	25-Vitamin D 3
HBeAg/Ab		NSE	FSH
Anti-HCV		SCC	Prolactin
		AFP	LH
		CEA	
		PSA	

Hepatitis

Thyroid

Tumor

Hormone  
s

**X3D**

**We Image** Your Needs.

[www.xddd.dk](http://www.xddd.dk)

# CorCam™

**SPECT Camera System**  
for Nuclear Cardiology Procedures



Golden Standard Cardiac SPECT

Prone & Supine Imaging

Seamless Workflow & Small Footprint

Fast Acquisition Time

Very Low Maintenance Cost

Made in Denmark

[www.xddd.dk](http://www.xddd.dk)



Follow us on LinkedIn



**uMI 550**  
Digital. Attainable.



**uMI Vista**  
Clarity. Profound.

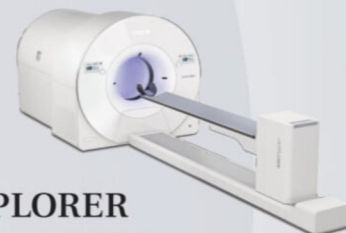


**uMI Panvivo**  
Empowering Tomorrow for All

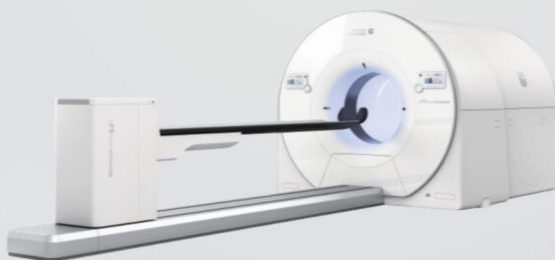


**uMI Panorama**  
Digital High-Resolution PET/CT.

PASSION FOR  
*Change*



**uEXPLORER**  
Total-body PET/CT.  
Born to EXPLORE.



**uMI Panorama GS**  
Next-Generation 148-cm  
Whole-Body PET/CT.

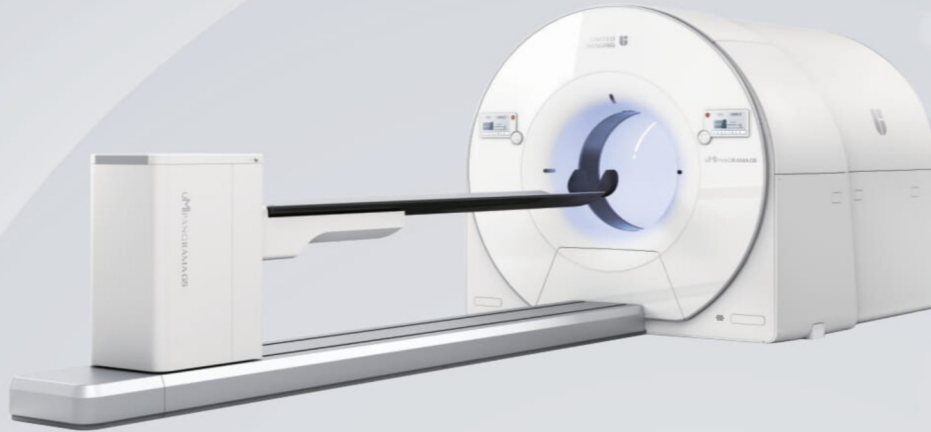


**uPMR 790**  
Next Generation. Now Realized.

Leading innovations in molecular imaging, United Imaging has developed a complete portfolio of LYSO-based digital SiPM PET detector systems. Dedicated to revolutionizing user experiences from clinical applications to advanced research, our portfolio starts where others end. Together with our global customers, we're changing how we view Molecular Imaging today, and in the future.

# uMI Panorama GS

Advancing Whole-Body Imaging



## Expanding Whole-Body Imaging with 148 cm AFOV

- 148 cm axial FOV enables single-bed whole-body imaging, covering key nuclear medicine regions from the skull to the knees with high sensitivity.
- 25x sensitivity gain ensures precise line-of-response capture for unparalleled imaging clarity and superior sensitivity for diverse imaging needs, including low-dose, rapid scans for pediatrics and brain imaging.
- Fits within the footprint of standard FOV PET/CT systems.

---

## Unlocking Precision without Compromise

- The 2.76 mm LYSO crystals provide a NEMA spatial resolution of 2.9 mm and 1.4 mm PSF+TOF spatial resolution with 100% SiPM coverage and ASIC technology, enabling sub-millimeter lesion detection and exceptional image clarity.
- Achieves 189 ps TOF and >3000 Peak-NECR, enhancing diagnostic accuracy with unparalleled details and contrast.
- AI-powered uExcel DPR and uExcel AIIR algorithms reduce noise and enhance contrast, while uExcel Focus corrects motion artifacts for improved quantification.

---

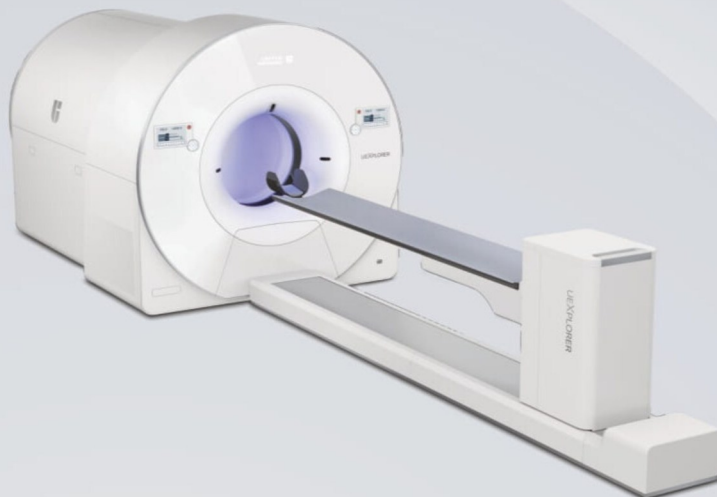
## Enabling a Panoramic View for New Clinical and Research Dimensions

- Delivers precise PET imaging with ultra-low radiation through CT-Free attenuation correction (AC), ensuring safety without compromising quality.
  - Supports advanced physiological and absolute quantitative analysis with innovative dynamic imaging technology (0.025/s Kernel Recon) and uKinetics.
  - Achieves high-speed online reconstruction with average static scan times under 3 minutes, with options for parallel reconstruction and redundant acquisition.
-



# uEXPLORER

Total-body PET/CT Born to Explore



## Unexplored Clinical Insight Became Tangible

- Industry-leading 194 cm single-bed AFOV for total-body coverage.
- The innovative cross-unit coincidence technology enables the capture of orders of magnitude more  $\gamma$  photons, giving a 40-fold overall sensitivity boost over conventional PET/CT systems.

---

## Game-changer – Exceptional Precision to Explore

- Achieves 2.9 mm NEMA spatial resolution for sub-millimeter lesion detection and enhanced diagnostic accuracy.
- 1024×1024 PET matrix provides unprecedented image contrast and detail.
- A 76 cm PET aperture enhances patient comfort during scans.

---

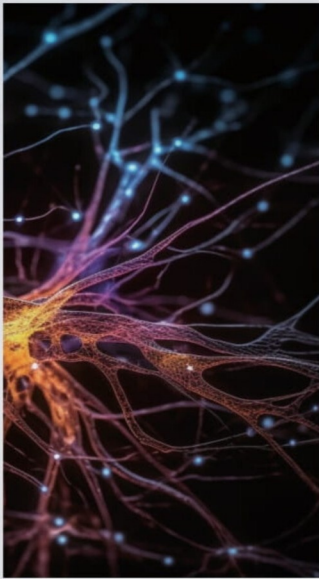
## Establish Total Body View for New Clinical and Research Dimensions

- Supports multifaceted research from diagnosis to theranostics for clinical complexity .
  - High count rate performance allows for better detail visualization, particularly for theranostics tracers such as  $^{68}\text{Ga}/^{90}\text{Y}$ .
  - Comprehensive research tools are provided for personalized needs, such as uKinetics, which supports total-body dynamic studies.
-



# uAI Solutions

uAI's multi-scenario solutions integrate multiple AI platforms and applications, building a digital healthcare ecosystem, and enabling precision clinical diagnosis and treatment. Furthermore, the integration of multiple AI technologies enables the entire process of diagnosis and treatment.



**uAI Solution for  
Neuroradiology**

ICH

Ischemic Stroke

Cerebral and Carotid Vessels

Cerebral CTP

Cerebral Collateral

PET/CT Neurology



**uAI Solution for  
Cardiology**

CCTA

FFRct

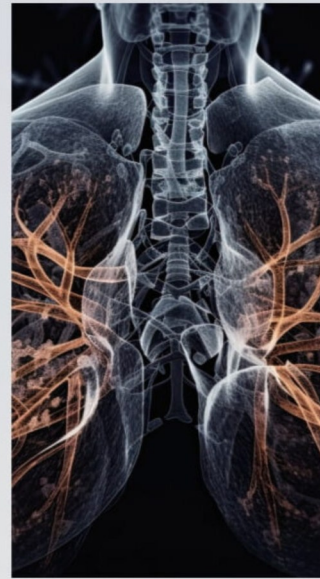
Coronary Plaque

Aortic Dissection

Coronary CS

Non-gated Coronary CS

CCTP



**uAI Solution for  
Thoracic Radiology**

Pulmonary Nodules

BMD

QCT Analysis

Bony Thorax Fractures

PE

Emphysema

Pneumonia

Lymph Nodes

Esophagus



**uAI Solution for Cancer  
Care  
Management**

Pulmonary Nodule 3D

Abdominal CT

PET/CT Oncology

# Clinical Outcomes of Patients Who Underwent Gallbladder Ultrasound and Cholescintigraphy For Acute Cholecystitis at St. Luke's Medical Center

Carl Joshua M. Chianpian , MD, Patricia Jarmin L. Pua, MD, Irene S. Bandong, MD

Department of Nuclear Medicine and Theranostics, St. Luke's Medical Center—Quezon City

E-mail address: joshchianpian@yahoo.com

## ABSTRACT

### **Background:**

*Acute cholecystitis is a severe inflammation of the gallbladder and is one of the most common causes of acute surgical abdomen. Ultrasonography and cholescintigraphy, are done in order to evaluate the presence or absence of inflammation of the gallbladder.*

### **Objective:**

*To determine clinical outcomes of adult patients who are suspected with acute cholecystitis who underwent both gallbladder ultrasound and cholescintigraphy scan.*

### **Methodology:**

*This is a cross-sectional analytical study of 38 patients who were admitted and had undergone both gallbladder ultrasound and cholescintigraphy scan. Chart review was done. Images of gallbladder ultrasound were reviewed independently by a radiologist who is blinded with the clinical data and scintigraphic findings. Images of the cholescintigraphy scan were reviewed independently by a nuclear medicine physician who was blinded with the clinical data and sonographic findings.*

### **Results:**

*Among the 38 patients, 13 patients (34%) had histopathological findings of acute cholecystitis. The mean age was 55.8 + 17.8 years and 52% were female. Of the 13 patients with acute cholecystitis, 8 patients (61%) had thickened gallbladder wall. Out of the 25 patients with no acute cholecystitis, 22 (88%) showed visualization of the gallbladder in 1 to 2 hours on cholescintigraphy scan with OR of 0.061 (95% CI: 0.0112 to 0.3271, p value 0.001). Out of the 38 patients, 8 patients (2 with acute cholecystitis and 6 without acute cholecystitis) had post-operative infection during the hospital stay.*

### **Conclusion:**

*The prevalence of acute cholecystitis was 34%. The incidence of post-operative infection was 21%. There is an association of scintigraphic finding of visualization of gallbladder in 1-2 hours among patients without acute cholecystitis.*

**Keywords:** Cholecystitis, HIDA, hepatobiliary iminodiacetic acid scan, ultrasound, cholescintigraphy

# INTRODUCTION

Acute cholecystitis is a severe inflammation of the gallbladder and is one of the most common causes of acute surgical abdomen. There are two types, namely acute acalculous cholecystitis and acute calculous cholecystitis, the latter being more common, occurring in 90% of all cases [1][2][3].

Part of the diagnosis and management relies on history, physical, laboratory and imaging examinations, which includes ultrasonography and cholescintigraphy, in order to evaluate the presence or absence of inflammation of the gallbladder.

Ultrasonography uses the principle of sound waves which are then analyzed to produce images of the body part being investigated. There have been multiple sonographic indicators described for acute cholecystitis including gallbladder wall thickness of more than 3mm, pericholecystic fluid, gallbladder distention, and sonographic Murphy's sign [4]. Different combination of these findings in order to diagnose acute cholecystitis has not been well established [3].

The most common indication for cholescintigraphy or hepatobiliary iminodiacetic (HIDA) scan is acute cholecystitis [5]. Cholescintigraphy is done by injecting a Technetium-99m labeled hepatobiliary radiopharmaceutical. Using a gamma camera, imaging of the hepatobiliary tree is then performed. Non-visualization or non-filling of the gallbladder on delayed imaging at 4 hours or 30 minutes after morphine infusion is diagnostic of acute cholecystitis [6].

There is wide variation in literature regarding the sensitivity and specificities of both modalities. The sensitivity and specificity of ultrasonography in detecting acute cholecystitis ranges from 26-88% and 80-88%, respectively while cholescintigraphy has a sensitivity of 96-97% and specificity of 90% [4][7]. One systematic review showed that cholescintigraphy demonstrated superior diagnostic accuracy than ultrasound, MRI, and CT scan in the detection of acute cholecystitis [7]. Furthermore, time from admission to surgery and length of hospital stay were longer for patients who underwent HIDA Scan [4]. Treatments include antibiotics, hydration and analgesia and ultimately, cholecystectomy or removal of the gallbladder [8].

Given the importance of accurate diagnosis in the treatment of acute cholecystitis, it is notable to

investigate which of these modalities carry significant weight in establishing or excluding diagnosis in order to better guide clinical decisions and improve patient outcomes.

## OBJECTIVE

### General Objective

To determine clinical outcomes of adult patients who are suspected with acute cholecystitis who underwent both gallbladder ultrasound (US) and hepatobiliary iminodiacetic acid (HIDA) scan.

### Specific Objectives

- To determine the clinical profile of adult patients with suspected acute cholecystitis who underwent gallbladder ultrasound and cholescintigraphy
- To determine the prevalence of acute cholecystitis among adult patients
- To determine the association of sonographic features of acute cholecystitis among adult patients
- To determine the association of scintigraphic features of acute cholecystitis among adult patients
- To determine the association of risk factors, sonographic and scintigraphic findings with in-hospital outcomes among adult patients

## METHODOLOGY

### Study Selection

All patients who underwent both gallbladder ultrasound and HIDA Scan between January 1, 2018 to and November 30, 2021 at St. Luke's Medical Center Quezon City or Global City.

### Inclusion Criteria

Aged 18 years old and above  
Undergone both gallbladder ultrasound and HIDA Scan in St. Luke's Medical Center Quezon City or Global City  
Admitted at St. Luke's Medical Center Quezon City or Global City

### Exclusion Criteria

Suboptimal sonographic images  
Pregnant patients  
Patients with history of morphine allergy  
Patients with incomplete data

### Sample Size Estimation

The prevalence of histologically proven acute cholecystitis with positive findings in both gallbladder ultrasound and HIDA scan was 66% with 80% reliability and 10% margin of error, the estimated sample size was 38 participants.[3]

### Data Collection

All eligible participants were to be anonymized by designation of subject numbers. Demographic data was gathered from the clinical abstract: age, sex, histopathology and follow-up.

### Data Extraction and Management

All patients who underwent both gallbladder ultrasound and HIDA between January 1, 2018 to and November 30, 2021 at St. Luke's Medical Center Quezon City and Global City were reviewed from the census of ultrasound section and nuclear medicine department. Chart review was done to all included participants.

### Ultrasound

Interpretation of the gallbladder sonographic images was done independently by two (2) radiologists with greater than 5 years of experience and were blinded on the patient's information, clinical consideration, as well as the HIDA scan findings. A third radiologist of similar years of experience, also blinded regarding the patient's information, clinical consideration, the HIDA scan findings and interpretation of the other 2 radiologists, evaluated the images in question to reach a consensus during the event of a non-agreement.

### HIDA scan

Evaluation of the HIDA images was done independently by two (2) nuclear medicine physicians of more than 5 years of experience who are blinded on the patient's information, clinical consideration, as well as the sonographic result. A third nuclear medicine physician of similar years of experience, also blinded regarding the patient's information, clinical consideration, the sonographic result, and the interpretation of the other 2 nuclear medicine physicians, evaluated the images in question to reach a consensus during the event of non-agreement.

### Operational definitions:

1. Ultrasound features of acute cholecystitis [9]:

- Thickened gallbladder wall – wall thickness of greater than 4mm in the setting of negative chronic liver disease/ascites or right-sided heart failure

- Enlarged gallbladder – long axis greater than 8 cm and short axis greater than 4 cm
- Sonolucent layer within the gallbladder wall
- Incarcerated gallbladder stone, debris echo and pericholecystic fluid collection
- Sonographic Murphy's sign – pain elicited when pressing the ultrasound probe in the right upper quadrant/gallbladder

2. Scintigraphic features of acute cholecystitis: non-visualization of the gallbladder at 4 hours of delayed imaging or 30 minutes after morphine infusion.
3. Suboptimal images – non-visualization of the gallbladder or contracted gallbladder on ultrasound
4. Acute cholecystitis - Clinical presentation of right upper quadrant pain and surgically proven acute cholecystitis or final clinical diagnosis based on ultrasound and/or HIDA Scan

### Study procedure and imaging protocol

Transabdominal ultrasound examination of the gallbladder was done using a low-frequency curvilinear probe.

HIDA imaging was done using a gamma camera with a low energy high resolution collimator where the dynamic images of the hepatobiliary system were acquired in the anterior and posterior views for 60 minutes at 15 seconds/frame after intravenous injection of 296 - 370 MBq (8-10 mCi) of Tc-99m disofenin/mebrofenin. Delayed imaging at 4 hours or post-morphine infusion (0.04 mg/kg diluted in 10 mL normal saline solution via slow injection for 2-3 minutes) imaging were done when needed.

### Statistical analysis

Descriptive statistics were used to summarize the demographic and clinical characteristics of the patients. Frequency and proportion were used for categorical variables, median and inter quartile range for non-normally distributed continuous variables and mean and standard deviation for normally distributed continuous variables. The Independent Sample T-test, Mann-Whitney U test and Fisher's exact/Chi-square test were used to determine the difference of mean, rank and frequency, respectively, between patients with and without Histopathology findings. Odds ratio and corresponding 95% confidence intervals from binary logistic regression was computed to determine significant predictors for Histopathology findings. All

statistical tests were two tailed tests. The Shapiro-Wilk test was used to test the normality of the continuous variables. Missing values were neither replaced nor estimated. Null hypotheses were rejected at 0.05 $\alpha$ -level of significance. STATA 13.1 was used for data analysis.

## RESULTS

Among the 38 participants included in the study, 13 patients (34%) were found to have histopathological findings consistent with cholecystitis, while the remaining 25 patients (66%) did not. The mean age of our sample population was  $55.79 \pm 17.83$  years. Both groups did not show a statistically significant difference in demographics such as age ( $p = 0.175$ ) and sex (Table 1). Out of the 13 patients diagnosed with cholecystitis, only 7 patients demonstrated sonographic Murphy's sign. Moreover, clinical symptoms of fever, nausea or vomiting were only present in 7 subjects, and only 4 of which were diagnosed with cholecystitis.

The ultrasound gallbladder findings were similar between both groups. The most common finding was a thickened gallbladder wall, observed in 60.53% of the total patient population, showing no statistical difference between the "With cholecystitis" and "Without cholecystitis" groups ( $p = 1.000$ ). Similarly, no significant differences were observed for the rest of the gallbladder ultrasound findings.

Serum amylase and lipase levels also did not differ significantly between the "With" and "Without" groups ( $p = 0.670$  and  $p = 0.450$ ), respectively. The patients who were clinically managed for cholecystitis had an average hospital stay of 4 days, while patients who were not diagnosed with cholecystitis stayed for an average of 2.5 days. This difference is also not statistically significant ( $p = 0.561$ ).

In-hospital outcome measures showed that there were 8 (21.05%) out of the 38 subjects who developed infection during confinement, 2 of which were related to cholecystitis.

Out of the 26 patients where the gallbladder was visualized after 1-2 hours on HIDA scan, 22 had no evidence of cholecystitis. This was a statistically significant finding ( $p\text{-value} < 0.01$ ), suggesting that visualization of the gallbladder after 1-2 hours on a HIDA scan is significantly associated with the absence of cholecystitis (Table 2). There were 12 patients with non-visualization of the gallbladder on HIDA scan after 4

hours or 30 minutes post-morphine administration. Of these 12 patients, 9 were histopathologically proven to have cholecystitis. Only 1 subject was observed to have a rim sign on HIDA scan and was eventually managed as a case of cholecystitis.

## DISCUSSION

For patients with acute abdominal pain, acute cholecystitis is responsible for 3-9% of hospitalizations. Ultrasound (US) is the preferred initial imaging modality for patients with suspected acute cholecystitis due to its lower cost and greater availability after hours. Cholescintigraphy has logistical challenges and is limited to providing information about the biliary tract, which restricts its use in clinical practice [10].

In this study, we determined the clinical outcomes of patients suspected with cholecystitis who underwent both US and HIDA scan. The sonographic and scintigraphic features of these patients were also correlated with their clinical profiles and risk factors.

We found no significant differences between the two groups across age, gender, presence of the sonographic Murphy's sign, clinical symptoms, gallbladder ultrasound findings and levels of serum amylase and lipase.

In-hospital outcomes showed that there were only 2 subjects in the "with cholecystitis" group who developed infection while the remaining 6 subjects who also developed infection were not diagnosed to have cholecystitis. Moreover, only 1 subject of the sample population was readmitted. These findings may be attributed to confounding factors during confinement that might come into play, particularly the presence of comorbidities and infection from other etiologies.

In a similar study by Rodriguez et al., wherein comparison between HIDA Scan and US were also used in the diagnosis of acute cholecystitis, it showed that HIDA scan was more superior in specificity and sensitivity than US, yielding the same results as our study. Their study also showed that patients who underwent US alone (4.3 days) had a shorter hospital stay than those who underwent HIDA Scan alone (6.7 days) [4]. Another study by Kamili et.al, showed that patient who underwent combined US and HIDA had an average of 4.7 days hospital stay [11]. When compared to our study, the overall length of hospital stay is shorter (average of 3 days) when using a combination of both US and HIDA Scan. A 1—2 day difference in the length of hospital stay

**TABLE 1.** Demographic and Clinical Profile of the Patients

	Histopathology findings			p-value
	Total	With Cholecystitis	Without Cholecystitis	
	Frequency (%); Mean ± SD; Median (IQR)			
Age (years)	55.79 ± 17.83	50.31 ± 20.33	58.64 ± 16.09	0.175
Sex				1.000
Male	18 (47.37)	6 (46.15)	12 (48)	
Murphy's sign				0.728
With	23 (60.53)	7 (53.85)	16 (64)	
Without	15 (39.47)	6 (46.15)	9 (36)	
Symptoms				
Fever	4 (10.53)	2 (15.38)	2 (8)	0.595
Vomiting	2 (5.26)	1 (7.69)	1 (4)	1.000
Nausea	1 (2.63)	1 (7.69)	0	0.342
Gallbladder ultrasound findings				
Thickened gallbladder wall	23 (60.53)	8 (61.54)	15 (60)	1.000
Intraluminal debris	19 (50)	6 (46.15)	13 (52)	1.000
Pericholecystic fluid	14 (36.84)	5 (38.46)	9 (36)	1.000
Sludge	14 (36.84)	6 (46.15)	8 (32)	0.486
Enlarged gallbladder				0.315
Amylase (U/L) (n=10)	58.6 (48 to 72)	58.6 (56 to 68)	58 (47 to 72)	0.670
Lipase (U/L) (n=20)	145.5 (101.5 to 191)	178.5 (119 to 194)	138 (85 to 154)	0.450
Clinical outcomes				
Infection (WBC >10,800 mm3)	8 (21.05)	2 (15.38)	6 (24)	0.689
Re-admission	1 (2.63)	1 (7.69)	0	0.342
Days of hospital stay, days	3 (1 to 11)	4 (2 to 11)	2.5 (1 to 10)	0.561
HIDA Impression				
Visualization of the gallbladder after 1 to 2 hours	26 (68.42)	4 (30.77)	22 (88)	0.001
Rim sign	1 (2.63)	1 (7.69)	0	0.342

**TABLE 2.** Factor associated with the occurrence of Histopathology findings

Parameter	Crude odds ratio	95% CI	p-value
Visualization of the gallbladder after 1 to 2 hours	0.0606	0.0112 to 0.3271	0.001

may be significant in our local setting. Furthermore, this study investigated which particular ultrasonographic and scintigraphic imaging findings in the diagnosis of cholecystitis will be an important factor in predicting the histopathologic findings. Herein, we observed that the visualization of the gallbladder (1 to 2 hours post HIDA) was significantly associated with the absence of cholecystitis (p-value = 0.001), making it an important parameter for evaluation of cholecystitis. Based on the clinical practice guidelines made by the Philippine college of Surgeons, the most accurate imaging test for acute cholecystitis is hepatobiliary scintigraphy, although for practical purposes, ultrasound is the appropriate initial imaging procedure [12]. This is also supported by a study by Velez et. al, that some surgeons consider HIDA scan to be the gold standard for the diagnosis of acute cholecystitis [13].

Overall, our results suggest that the HIDA scan is more sensitive in the diagnosis of patients suspected of cholecystitis. Meanwhile, ultrasound, though less sensitive, proved more helpful in detecting other gallbladder findings such as gallbladder wall thickening, enlarged gallbladder, presence of pericholecystic fluid, cholelithiasis, and bile sludge. Another pertinent finding in our study was the presence of sonographic Murphy's sign that was noted in both "with cholecystitis" and "without cholecystitis" group. However, it might be noteworthy that this finding was found more in the "without cholecystitis" group (64%) than in the "with cholecystitis" (53.85%) group, which is supported by a study of Bree, that the sonographic Murphy's sign yielded a lot of false positive results, making this sign less reliable for cholecystitis [14].

The level of agreement between the two (2) radiologists and (2) nuclear medicine physicians were in concordance. However, there is a relative lack of concordance between the radiologists and the nuclear medicine physicians. Operator expertise, dependence, and subjectivity may also be contributing factors into the discordance but may be eventually diminished with experience.

#### **LIMITATION OF THE STUDY**

The research paper's generalizability may be limited by its setting in a tertiary hospital, which serves a patient population disproportionately comprised of individuals from social classes A and B. Due to ultrasound being an operator dependent imaging modality, the quality of the images may vary depending on the skills of the operator. In addition, other factors like patient cooperation and patient's body habitus may also affect the images at the

time of scanning [3].

## **CONCLUSION**

In conclusion, the prevalence of acute cholecystitis was 34%. The incidence of post-operative infection was 21%. There is a statistically significant association of scintigraphic visualization of the gallbladder after 1-2 hours and the absence of acute cholecystitis. This suggests that HIDA scan plays a role in the preoperative diagnosis of acute cholecystitis, and therefore, its utilization should be encouraged, especially when ultrasound findings are inconclusive. HIDA Scan along with US may possibly reduce the average hospital stay of the patient compared to either using the HIDA scan alone or using US alone.

Overall, our findings could aid in the clinical evaluation of patients being suspected for cholecystitis with an impact on hospital stay and potentially, the time to surgery.

#### **Acknowledgements**

The authors would like to express their gratitude to the following:

1. To Dr. Katleya Theresa G. Manlapaz and Dr. Cursill P. Ibay for participating in this study as our radiologist readers of this study.
2. To the staff of the St. Luke's Medical Center Information Management Department, for their significant contribution in retrieving all available images during data collection of this study.

## **REFERENCES**

1. Klein, Jeffrey, et al. Brant and Helms' Fundamentals of Diagnostic Radiology. Lippincott Williams & Wilkins, 2018.
2. Montini, K. M., & Tulchinsky, M. (2015). Applied hepatobiliary scintigraphy in acute cholecystitis. *Applied Radiology*, 44(5), 21-30. <https://doi.org/10.37549/ar2183>.
3. Kaoutzanis, C., Davies, E., Leichtle, S. W., Welch, K. B., Winter, S., Lampman, R. M., & Arneson, W. (2014). Abdominal ultrasound versus hepato-imino diacetic acid scan in diagnosing acute cholecystitis--what is the real benefit?. *The Journal of surgical research*, 188(1), 44–52. <https://doi.org/10.1016/j.jss.2014.01.004>.
4. Rodriguez, L. E., Santaliz-Ruiz, L. E., De La Torre-Bisot, G., Gonzalez, G., Serpa, M. A., Sanchez-Gaetan, F., Martinez-Trabal, J. L., Peguero-Rivera, J. A., & Bolanos-Avila, G. (2016). Clinical implications of hepatobiliary scintigraphy and ultrasound in the diagnosis of acute cholecystitis. *International journal of surgery (London, England)*, 35, 196–200. <https://doi.org/10.1016/j.ijsu.2016.09.084>

5. Ziessman H. A. (2010). Nuclear medicine hepatobiliary imaging. *Clinical gastroenterology and hepatology : the official clinical practice journal of the American Gastroenterological Association*, 8(2), 111–116. <https://doi.org/10.1016/j.cgh.2009.10.017>.
6. O'Malley, Janis, et al. (2020). *Nuclear Medicine and Molecular Imaging: The Requisites* (5th ed.) 568-569.
7. Kiewiet, J. J., Leeuwenburgh, M. M., Bipat, S., Bossuyt, P. M., Stoker, J., & Boermeester, M. A. (2012). A systematic review and meta-analysis of diagnostic performance of imaging in acute cholecystitis. *Radiology*, 264(3), 708–720. <https://doi.org/10.1148/radiol.12111561>.
8. Mujoondar, M., Russell, E., Dionne, F., Moulton, K., Murray, C., McGill, S., & Lambe, K. (2012). *Optimizing Health System Use of Medical Isotopes and Other Imaging Modalities*. Canadian Agency for Drugs and Technologies in Health.
9. Hirota, M., Takada, T., Kawarada, Y., Nimura, Y., Miura, F., Hirata, K., Mayumi, T., Yoshida, M., Strasberg, S., Pitt, H., Gadacz, T. R., de Santibanes, E., Gouma, D. J., Solomkin, J. S., Belghiti, J., Neuhaus, H., Büchler, M. W., Fan, S. T., Ker, C. G., Padbury, R. T., ... Dervenis, C. (2007). Diagnostic criteria and severity assessment of acute cholecystitis: Tokyo Guidelines. *Journal of hepato-biliary-pancreatic surgery*, 14(1), 78–82. <https://doi.org/10.1007/s00534-006-1159-4>.
10. Bernescu, I., Eng, O., Potdevin, L., Monteiro, R., Mino, J., Chang, E., & Davidov, T. (2013). Is HIDA Scan Necessary for Sonographically Suspicious Cholecystitis?. *Journal Of Current Surgery*, 3(2), 62-65.
11. Kalimi, R., Gecelter, G., Caplin, D., Brickman, M., Tronco, G., Love, C., Yao, J., Simms, H. S., & Marini, C. P. (2001). Diagnosis of acute cholecystitis: sensitivity of sonography, cholescintigraphy, and combined Sonography-Cholescintigraphy. *Journal of the American College of Surgeons*, 193(6), 609–613. [https://doi.org/10.1016/s1072-7515\(01\)01092-4](https://doi.org/10.1016/s1072-7515(01)01092-4).
12. Bongala, D. S., Santos, R. M. F., Panaligan, M. M., de los Santos, N. C., Rigor, M., Brillantes, M., & Anastacio, A. L. (2009). *PCs. Evidence-Based Clinical Practice Guidelines On The Diagnosis And Treatment Of Cholecystitis*. <https://pcs.org.ph/wp-content/uploads/2022/03/EBCPG-chole.pdf>.
13. Romero-Velez, G., Pereira, X., Mandujano, C. C., Parides, M. K., Muscarella, P., Melvin, W. S., Love, C., & McAuliffe, J. C. (2021). The Utility of Hepatobiliary Scintigraphy Scans in the Tokyo Guidelines Era for Acute Cholecystitis. *The Journal of surgical research*, 268, 667–672. <https://doi.org/10.1016/j.jss.2021.08.009>.
14. Bree R. L. (1995). Further observations on the usefulness of the sonographic Murphy sign in the evaluation of suspected acute cholecystitis. *Journal of clinical ultrasound : JCU*, 23(3), 169–172. <https://doi.org/10.1002/jcu.1870230304>.

# Taking the Lead in PET/CT Imaging and Innovative Radiopharmaceuticals



## [18F]-FDG

A sugar analog used to detect **metabolically active malignant lesions**.  
A non-invasive approach to accurate diagnosis and staging for the optimal management of cancer patients

## [18F]-FBB

Developed for routine clinical application to visualize beta amyloid neuritic plaque density.  
An effective tool to **differentiate Alzheimer's Disease** from other forms of Dementia

## [18F]-FPSMA

Named as a top medical innovation by Cleveland Clinic in 2022. PSMA PET scan has greater sensitivity and can detect **prostate cancer metastases** sooner, allowing clinicians to better serve patients and make treatment decisions

## [177Lu]-LuPSMA

Partnered with PSMA-directed PETCT scan, LuPSMA offers a **Theranostic approach** to treatment of metastatic castration-resistant prostate cancer (mCRPC)



**NATIONAL KIDNEY AND TRANSPLANT INSTITUTE**  
East Ave., Diliman Quezon City



**CENTURIA PET/CT CENTER**  
G/F Centuria Medical Makati, Kalayaan Ave., Cpr. Salamanca, Makati City



**AUF MEDICAL CENTER**  
Angeles City, Philippines

**ManilaMedo**  
MOUNT GRACE HOSPITAL  
850 United Nations Ave, Paco, Manila



**MARY MEDIATRIX MEDICAL CENTER**  
THE HUB OF HEALTHCARE EXPERTS  
J.P. Laurel Highway, Lipa City Batangas



**CAREVIEW Cancer Center BGC**  
31st Street Cor. Second Ave., Crescent Park West, BGC



**Philippine General Hospital**  
Taft Ave, Ermita, Manila



**CAREVIEW Cancer Center**  
SM Valenzuela  
McArthur Highway, Brgy. Karuhatan, Valenzuela City



**PET/CT PATIENT SUPPORT**

+63 998 323 5425  
+63 917 714 4248  
+63 917 714 4266  
[patientsupport@khealthcorp.com](mailto:patientsupport@khealthcorp.com)

SCAN THE QR CODE



PET/CT FINANCIAL ASSISTANCE

NEED A PET/CT SCAN?



Schedule it with us.  
Let CARE CALL Team call you

# A Comparative Study of Automated Quantitative and Clinical Visual Analysis of Myocardial Viability among Adult Patients with CAD using Rest-Redistribution Thallium-201 Gated SPECT-MPI

Mary Amie Gelina E. Dumatol, MD, Angelo O. Martinez, MD, Michele D. Ogbac, MD

Nuclear Medicine Division, Philippine Heart Center

E-mail address: medumatol@alum.up.edu.ph

## ABSTRACT

### **Introduction:**

*Myocardial perfusion imaging (MPI) is integral in the assessment of myocardial viability. Interpretation of MPI studies is usually done through visual analysis by physician readers, though automated parameters by cardiac software may contribute objective information. Studies comparing visual and automated analysis are limited.*

### **Objective:**

*Our aim is to compare automated quantitative analysis and clinical visual analysis in the assessment of myocardial viability using rest-redistribution thallium-201 gated SPECT-MPI.*

### **Methodology:**

*We studied adult patients who underwent rest-redistribution thallium-201 SPECT MPI. Automated parameters of myocardial perfusion and left ventricular function, namely initial rest scores (rest SS), delayed redistribution scores (redistribution SS), summed difference scores (SDS), summed motion scores (SMS), and summed thickening scores (STS) were derived using the Cedars-Sinai Cardiac Suite for both noncorrected (NC) and attenuation corrected (AC) data sets. Semiquantitative scoring was done through visual analysis by two expert readers. Statistical analysis was performed to examine the differences between the two.*

### **Results:**

*A total of 49 patients were included. Statistically significant differences were seen between visual (averaged between two readers) and automated perfusion scores for NC rest SS ( $p < 0.001$ ), redistribution SS ( $p = 0.026$ ), and SDS ( $p < 0.001$ ). Improved comparability was observed with the AC images, with a significant difference between visual and automated parameters only seen for SDS ( $p = 0.018$ ). Good comparability with no significant difference was demonstrated between visual and automated analysis of both LV motion ( $p = 0.566$ ) and thickening ( $p = 0.190$ ).*

### **Conclusion:**

*Visual analysis remains an integral part of SPECT MPI interpretation, given significant differences that were observed between it and automated analysis, particularly with regards to myocardial perfusion. Automated analysis of perfusion and LV function can be used alongside visual assessment to address inter-reader variability.*

**Keywords:** *myocardial perfusion imaging (MPI), thallium-201, myocardial viability, automated quantification, reader variability, Cedars-Sinai Quantitative Perfusion SPECT / Quantitative Gated SPECT (QPS/QGS), SPECT-CT*

# INTRODUCTION

Myocardial viability assessment is a vital part of the management of coronary artery disease, aiding in the determination of whether a patient may benefit from revascularization [1], with the goal of improving quality of life and overall prognosis. Myocardial perfusion imaging (MPI) using gated single photon emission computed tomography (SPECT) has long been used for the assessment of myocardial viability [2]. While positron emission tomography (PET) imaging with F-18 fluorodeoxyglucose (F-18 FDG), especially when combined with perfusion imaging, has emerged as the current standard [3], its use in current practice continues to be limited due to issues with costs and availability. As such, SPECT-MPI still plays a significant role in viability studies, with the added information regarding wall motion and thickening improving its accuracy to become comparable with the PET standard [4].

Clinical visual analysis remains the recommended method for interpretation of gated SPECT-MPI studies. However, technological advancements throughout the years have led to the development of software programs that enable automated quantification of such imaging studies, allowing an objective and more reproducible way of assessment [3].

Readings produced by these quantitative measures have been shown to be comparable with traditional visual analysis by physician interpreters in the diagnosis of coronary artery disease (CAD) [5][6]. However, studies incorporating data on both perfusion and gated motion as well as focusing on how automated assessment of myocardial viability compares to expert reading remain scarce, even more so in the high-risk population unable to undergo stress imaging protocols.

## OBJECTIVE

This study's objective therefore is to compare automated quantitative analysis and clinical visual analysis in the assessment of myocardial viability using rest-redistribution thallium-201 gated SPECT-MPI.

## METHODOLOGY

This retrospective cross-sectional study included 49 adult patients with known coronary artery disease, who underwent rest-redistribution thallium-201 SPECT-MPI between January 1, 2019 and December 31, 2020.

Systematic random sampling was done to complete the sample population. Patients were excluded if clinical data was incomplete, scans were suboptimal, and/or percutaneous coronary intervention (PCI) and/or coronary artery bypass graft (CABG) surgery had been done.

This study was granted approval by the Technical Review Committee and the Institutional Ethics Review Board of the Philippine Heart Center.

### Image Acquisition and Processing

All patients included in this study underwent viability assessment using a one-day rest-redistribution thallium-201 gated SPECT-MPI protocol. Fasting was done for four hours prior to the procedure. Baseline electrocardiograph, blood pressure, and heart rate were recorded prior to the administration of 111 MBq (3 mCi) of thallium-201 via intravenous port bolus. Gated SPECT images at rest were acquired, while redistribution images were obtained after a 4-hour interval. Imaging was done using a dual-head hybrid SPECT/CT system (Discovery NM/CT 670 ES, GE Healthcare), equipped with a low-energy high resolution (LEHR) collimator.

### Automated Analysis

Automated parameters of myocardial perfusion, wall motion, and systolic thickening for each imaging study was obtained using the Quantitative Perfusion SPECT / Quantitative Gated SPECT software (QPS/QGS, Cedars-Sinai Medical Center, Los Angeles, California, USA) with the vendor-provided normal database for resting thallium. Initial summed scores (rest), delayed summed scores (redistribution), summed difference scores (SDS), summed wall motion scores (SMS), and summed thickening scores (STS) were derived from the automated analysis.

### Visual Analysis

Image interpretation was done independently by two nuclear medicine physicians of more than 10 years of experience. Both readers were initially blinded to the automated quantification measures generated by the software as well as other available work-up information. Limited clinical data, including the patient's sex, age, height, weight, and symptoms at the time of scan, were provided as these directly affected scan reading.

The American Heart Association (AHA) 17-segment model was used in image interpretation. Perfusion defects were graded with the use of a 5-point system ranging from 0 (normal) to 4 (absent uptake). Noncorrected (NC) and attenuation corrected (AC) scan

images were scored separately. Visual analysis of left ventricular function was conducted using grading scales for segmental wall motion (scale of 0-5) and systolic thickening (scale of 0-3).

A detailed description of the methodology used can be found in Appendix A.

### Sample Size

A minimum of 47 patients was required for this study based on 79.81% total agreement of automated summed scores versus the visual scan interpretation [5], 5% level of significance and 11.5% desired half-width of the confidence interval [7].

### Statistical Analysis

Descriptive statistics was used to summarize the demographic and clinical characteristics of the patients. Frequency and proportion were used for categorical variables, median and inter quartile range for non-normally distributed continuous variables, and mean and SD for normally distributed continuous variables. Signed rank test was used to determine the difference between the two readers as well as the automated perfusion result. All statistical tests were two tailed tests. Shapiro-Wilk test was used to test the normality of the continuous variables. Missing values were neither replaced nor estimated. Null hypotheses were rejected at 0.05 $\alpha$ -level of significance. STATA 13.1 was used for data analysis.

## RESULTS

### Patient Characteristics

A total of 49 patients were included in the final study. Table 1 summarizes the baseline characteristics of these patients.

### Automated and Visual Analysis

Comparison of visual (averaged between two expert readers) and automated scores of perfusion showed significant differences for noncorrected rest summed scores ( $p < 0.001$ ), redistribution summed scores ( $p = 0.026$ ), and summed difference scores ( $p < 0.001$ ) (Table 2). Comparability was better with analysis of the attenuation corrected images with a significant difference between visual scoring and automated parameters only seen for SDS ( $p = 0.018$ ). No significant difference was seen between visually scored and software-derived rest SS ( $p = 0.073$ ) and redistribution SS ( $p = 0.774$ ) in the attenuation correction data set.

Gated data analysis showed good comparability with no significant difference demonstrated between visual and

automated analysis of both LV motion ( $p = 0.566$ ) and thickening ( $p = 0.190$ ).

**TABLE 1.** Patient population baseline characteristics (n=49)

Characteristic	Frequency (%) Mean $\pm$ SD
Age, years	59.57 $\pm$ 9.6
Sex	
Male	43 (87.76)
Female	6 (12.24)
Weight, kg	65.41 $\pm$ 10.25
Height, cm	163.73 $\pm$ 7.26
Body mass index	24.37 $\pm$ 3.34
Coronary Angiography result	
1-vessel disease (1VD)	7 (14.29)
2-vessel disease (2VD)	9 (18.37)
3-vessel disease (3VD)	33 (67.35)
<b>Risk Factors for CAD</b>	
Hypertension	37 (75.51)
Dyslipidemia	30 (61.22)
Diabetes mellitus	9 (18.37)
Smoking History	23 (46.94)
<b>Past Medical History</b>	
Myocardial Infarction	42 (85.71)
Cerebrovascular Disease (CVD)	2 (4.08)
<b>Symptomatology</b>	
Chest pain	
None	24 (48.98)
Nonspecific	14 (28.57)
Atypical	5 (10.20)
Typical	6 (12.24)
Exertional dyspnea	29 (59.18)
Easy fatigability	26 (53.06)
Orthopnea	5 (10.20)

**TABLE 2.** Comparison of visual reading and automated analysis

	Reader 1 & 2	Automated	p-value
	Median (IQR)		
Perfusion			
NC			
Rest SS	23 (15 to 31)	14 (9 to 21)	< 0.001
Redistribution SS	21 (11 to 27)	14 (9 to 25)	0.026
SDS	0 (0 to 5)	-1 (-3 to 3)	< 0.001
AC			
Rest SS	18 (9 to 24)	14 (7 to 21)	0.073
Redistribution SS	14 (8 to 22)	14 (9 to 19)	0.774
SDS	0 (0 to 3)	0 (-2 to 3)	0.018
Gated (LV Function)			
SMS	43 (22 to 52)	37 (29 to 48)	0.566
STS	25 (17 to 34)	29 (20 to 32)	0.190

## DISCUSSION

Our study compared automated quantitative analysis and clinical visual analysis in the assessment of myocardial viability using rest-redistribution thallium-201 gated SPECT-MPI. Statistically significant differences were demonstrated between visual analysis and software-derived parameters of myocardial perfusion in terms of rest summed scores, redistribution summed scores, and summed difference scores (SDS) for the noncorrected (NC) data set. Improved comparability was seen with the attenuation corrected (AC) data. Good comparability was demonstrated between visual and automated analysis for gated parameters of LV function, with both summed wall motion scores (SMS) and summed thickening scores (STS) showing no significant difference between the two.

SPECT-MPI is still among the most commonly used modalities for cardiac viability assessment, largely due to its wider availability and cost-effectiveness [2]. In our institution, MPI using the rest-redistribution protocol with thallium-201 is particularly of use in patients wherein viability assessment is essential but factors such as clinical state and physical status do not make stress testing either with exercise or pharmacologic agents a feasible option.

While visual analysis by physician readers is still the widespread method in use for interpreting MPI studies,

technological advancements have led to the emergence of several software programs that are capable of producing automated measures of perfusion and left ventricular function [8][9][10] with the aim of enabling more objective and precise assessments. These software programs have been individually validated and shown to be highly reproducible, potentially addressing the inherent experience and skill-dependent limitations of visual analysis [11]. Automated analysis makes use of normal databases [12], composed of perfusion and gated data from persons with a low probability for coronary artery disease (CAD), to which patient data is compared and contrasted. Applied normal databases are often specific to sex, radiopharmaceutical used, imaging protocol, and positioning during imaging. Custom normal databases may also be constructed and used in place of those provided by the software vendor and developer.

Past studies comparing visual readings by physician experts and automated analysis by cardiac software programs for the diagnosis of CAD generally show high correlation between the two [5][13][14]. These studies focused only on NC data and made use only of the normal databases included with the software. In the study by Arsanjani et al. [6], using coronary angiography results as the gold standard, automated parameters were shown to be at least equivalent to visual analysis at a per-patient basis, with attenuation correction showing improved accuracy of automated analysis. In connection, comparability between visual and automated analysis

was observed to be improved in our study, particularly with the rest and redistribution scores, with AC, compared to NC.

Meanwhile, the study of Driessen et al. [15] showed comparable performance of automated and visual analysis using their constructed institutional normal database, but not with the vendor-provided database, which when used, showed better concordance of visual readings with fractional flow reserve-detected CAD compared with the automated indices. The patients included in the default database may have varied much in terms of body composition with the patients seen in their institution; hence, the difference in performance. Studies looking into the effect of a custom populations-specific normal database, however, have been met with conflicting results with some showing significant differences with default vendor-provided databases [16] [17][18] and others showing comparability [19][20]. A population-based normal database has yet to be made in the Philippines, and the effect of such a database is still unclear at present.

In contrast to the results for perfusion indices, no significant differences were observed between visual and automated analysis of left ventricular function. Interestingly, visual scoring by the two expert readers also showed good comparability for both wall motion and thickening. The automated analysis of wall motion and thickening has previously been shown to perform better for CAD detection compared to visual analysis [21]. However, while centers performing MPI frequently report derived ejection fraction and left ventricular volumes, measured quantified indices for wall motion and thickening continue to be seldom utilized [2] in favor of descriptive reports based on visual observation.

Notably, our study demonstrated significant variability of perfusion scoring between physician readers, particularly for the summed difference scores (SDS). The SDS represents what is termed to as 'resting ischemia' using the rest-redistribution thallium MPI protocol, reflecting the degree of viable myocardium [22]. The limited studies on inter-reader variability in myocardial perfusion imaging show mixed results with some showing good agreement [23][24], and others poor agreement between readers [25]. Visual interpretation of diagnostic medical images is inherently subjective and variable, affected by factors such as reader experience, fatigue, reading environment, stress levels, and internal biases. [26] Even among expert readers with considerable years of experience, disagreements may

still occur, especially in challenging cases that fall within the borderline of multiple possibilities. This inherent variability, as reflected in our findings, highlights the need for more objective ways of assessment to improve diagnostic study reporting, potentially in the form of computer-aided automated analysis.

Our study has a number of limitations. We made use of a single cardiac software (QPS/QGS) in the automated analysis and because considerable differences can occur between software [27][28], the degree of comparability of indices derived by another software program with respect to visual analysis may not be the same as what we have observed in this study. Furthermore, this was a single center study and while minimal manual intervention was done for the automated analyses, there may still be variations in protocol, scanning technique, and processing across institutions, which may affect derived values. Finally, no gold standard was used in the direct comparison of visual and automated analyses for myocardial viability assessment. Future work exploring accuracy through comparison with F-18 FDG PET imaging can be explored, though this modality may also be subject to reader variability as well as possess its own limitations.

The existing and continually evolving cardiac software programs for SPECT MPI, with their ability to produce automated parameters of perfusion and left ventricular function, have the potential to address inter-reader variability. However, given significant differences that were observed between automated and visual analysis, the latter remains an irreplaceable and integral part of SPECT MPI interpretation, particularly with regards to perfusion. We recommend using automated analysis alongside in combination with visual assessment, especially when addressing equivocal cases that may cause reader dispute and to assist nuclear medicine physicians and nuclear cardiologists in the beginning of their training.

## CONCLUSION

Automated indices of left ventricular wall motion and thickening are comparable with expert reader scoring. Though significant differences still remain, the addition of attenuation correction improves the comparability of perfusion parameters with that of visual analysis. Automated analysis of perfusion and left ventricular function can be used alongside visual assessment for myocardial viability to potentially address inter-reader

## Acknowledgment

The authors would like to thank Mr. Rhalp Jaylord Valenzuela for his valuable statistical inputs, and the staff members of the Philippine Heart Center Nuclear Medicine Division, especially Mr. Alvin Antonio Villalon, for the assistance and support that led to the completion of this research project.

## REFERENCES

1. Jamiel, A., Ebid, M., Ahmed, A. M., Ahmed, D., & Al-Mallah, M. H. (2017). The role of myocardial viability in contemporary cardiac practice. *Heart failure reviews*, 22(4), 401–413. <https://doi.org/10.1007/s10741-017-9626-3>.
2. Garcia, M. J., Kwong, R. Y., Scherrer-Crosbie, M., Taub, C. C., Blankstein, R., Lima, J., Bonow, R. O., Eshtehardi, P., Bois, J. P., & American Heart Association Council on Cardiovascular Radiology and Intervention and Council on Clinical Cardiology (2020). State of the Art: Imaging for Myocardial Viability: A Scientific Statement From the American Heart Association. *Circulation. Cardiovascular imaging*, 13(7), e000053. <https://doi.org/10.1161/HCI.0000000000000053>.
3. Garcia, E. V., Slomka, P., Moody, J. B., Germano, G., & Ficaro, E. P. (2019). Quantitative Clinical Nuclear Cardiology, Part 1: Established Applications. *Journal of nuclear medicine : official publication, Society of Nuclear Medicine*, 60(11), 1507–1516. <https://doi.org/10.2967/jnumed.119.229799>.
4. Zhang, F., Wang, J., Shao, X., Yang, M., Qian, Y., Yang, X., Wu, Z., Li, S., Xin, W., Shi, Y., Liu, B., Yu, W., He, Z., Zhou, W., & Wang, Y. (2021). Incremental value of myocardial wall motion and thickening to perfusion alone by gated SPECT myocardial perfusion imaging for viability assessment in patients with ischemic heart failure. *Journal of nuclear cardiology : official publication of the American Society of Nuclear Cardiology*, 28(6), 2545–2556. <https://doi.org/10.1007/s12350-020-02040-4>.
5. Leslie, W. D., Tully, S. A., Yogendran, M. S., Ward, L. M., Nour, K. A., & Metge, C. J. (2004). Automated quantification of 99mTc sestamibi myocardial perfusion compared with visual analysis. *Nuclear medicine communications*, 25(8), 833–838. <https://doi.org/10.1097/01.mnm.0000133075.72292.53>.
6. Arsanjani, R., Xu, Y., Hayes, S. W., Fish, M., Lemley, M., Jr, Gerlach, J., Dorbala, S., Berman, D. S., Germano, G., & Slomka, P. (2013). Comparison of fully automated computer analysis and visual scoring for detection of coronary artery disease from myocardial perfusion SPECT in a large population. *Journal of nuclear medicine : official publication, Society of Nuclear Medicine*, 54(2), 221–228. <https://doi.org/10.2967/jnumed.112.108969>.
7. Peacock JL, Peacock PJ. Research design. (ed). Oxford handbook of Medical Statistics. United States: Oxford University Press; 2011. pp. 60-61.
8. Germano, G., Kavanagh, P. B., Slomka, P. J., Van Kriekinge, S. D., Pollard, G., & Berman, D. S. (2007). Quantitation in gated perfusion SPECT imaging: the Cedars-Sinai approach. *Journal of nuclear cardiology : official publication of the American Society of Nuclear Cardiology*, 14(4), 433–454. <https://doi.org/10.1016/j.nuclcard.2007.06.008>.
9. Ficaro, E. P., Lee, B. C., Kritzman, J. N., & Corbett, J. R. (2007). Corridor4DM: the Michigan method for quantitative nuclear cardiology. *Journal of nuclear cardiology : official publication of the American Society of Nuclear Cardiology*, 14(4), 455–465. <https://doi.org/10.1016/j.nuclcard.2007.06.006>.
10. Garcia, E. V., Faber, T. L., Cooke, C. D., Folks, R. D., Chen, J., & Santana, C. (2007). The increasing role of quantification in clinical nuclear cardiology: the Emory approach. *Journal of nuclear cardiology : official publication of the American Society of Nuclear Cardiology*, 14(4), 420–432. <https://doi.org/10.1016/j.nuclcard.2007.06.009>.
11. Sanghani, R. M., & Doukky, R. (2018). Fully automated analysis of perfusion data: The rise of the machines. *Journal of nuclear cardiology : official publication of the American Society of Nuclear Cardiology*, 25(4), 1361–1363. <https://doi.org/10.1007/s12350-017-0884-1>.
12. Rubeaux, M., Xu, Y., Germano, G., Berman, D. S., & Slomka, P. J. (2016). Normal Databases for the Relative Quantification of Myocardial Perfusion. *Current cardiovascular imaging reports*, 9, 22. <https://doi.org/10.1007/s12410-016-9385-x>.
13. Doğan, C., Çınaral, F., Karagöz, A., Bayram, Z., Önal, S. Ç., Candan, Ö., Acar, R. D., Çap, M., Erdoğan, E., Hakkör, A., Akbal, Ö. Y., Uslu, A., Kaymaz, C., & Özdemir, N. (2019). Comparison of automated quantification and semiquantitative visual analysis findings of IQ SPECT MPI with conventional coronary angiography in patients with stable angina. *Konvansiyonel koroner anjiyografi ile IQ-SPECT kullanılarak yapılan otomatik ve görsel analiz yönteminin kararlı anjinalı hastalarda karşılaştırılması. Turk Kardiyoloji Dernegi arsivi : Turk Kardiyoloji Derneginin yayın organidir*, 47(5), 357–364. <https://doi.org/10.5543/tkda.2019.03367>.
14. Angelidis, G., Valotassiou, V., Tsougos, I., Tzavara, C., Psimadas, D., Theodorou, E., Ziaka, A., Giannakou, S., Ziangas, C., Skoularigis, J., Triposkiadis, F., & Georgoulas, P. (2022). Automated Analysis vs. Expert Reading in Nuclear Cardiology: Correlations with the Angiographic Score. *Medicina (Kaunas, Lithuania)*, 58(10), 1432. <https://doi.org/10.3390/medicina58101432>.
15. Driessen, R. S., Raijmakers, P. G., Danad, I., Stuijzand, W. J., Schumacher, S. P., Leipsic, J. A., Min, J. K., Knuuti, J., Lammertsma, A. A., van Rossum, A. C., van Royen, N., Underwood, S. R., & Knaapen, P. (2018). Automated SPECT analysis compared with expert visual scoring for the detection of FFR-defined coronary artery

- European journal of nuclear medicine and molecular imaging, 45(7), 1091–1100. <https://doi.org/10.1007/s00259-018-3951-1>
16. Nakajima, K., Okuda, K., Kawano, M., Matsuo, S., Slomka, P., Germano, G., & Kinuya, S. (2009). The importance of population-specific normal database for quantification of myocardial ischemia: comparison between Japanese 360 and 180-degree databases and a US database. *Journal of nuclear cardiology : official publication of the American Society of Nuclear Cardiology*, 16(3), 422–430. <https://doi.org/10.1007/s12350-009-9049-1>.
  17. Hosseini, A., Fattahi, M. R., Mehrpooya, M., Khosravi, A., Farzanefar, S., Abbasi, M. (2023). Normal perfusion and function myocardial perfusion imaging indices in Iranian normal females. *Iranian Journal of Nuclear Medicine*, 31 (1): 29-34. doi: 10.22034/irjnm.2022.40036.
  18. Cuberas-Borrós, G., Aguadé-Bruix, S., Boronat-de Ferrater, M., Muxí-Pradas, M. A., Romero-Farina, G., Castell-Conesa, J., Aliaga, V., García-Dorado, D., & Candell-Riera, J. (2010). Normal myocardial perfusion SPECT database for the Spanish population. *Revista espanola de cardiologia*, 63(8), 934–942. [https://doi.org/10.1016/s1885-5857\(10\)70187-0](https://doi.org/10.1016/s1885-5857(10)70187-0).
  19. Wolak, A., Slomka, P. J., Fish, M. B., Lorenzo, S., Acampa, W., Berman, D. S., & Germano, G. (2008). Quantitative myocardial-perfusion SPECT: comparison of three state-of-the-art software packages. *Journal of nuclear cardiology : official publication of the American Society of Nuclear Cardiology*, 15(1), 27–34. <https://doi.org/10.1016/j.nuclcard.2007.09.020>.
  20. Guner, L. A., Karabacak, N. I., Cakir, T., Akdemir, O. U., Kocaman, S. A., Cengel, A., & Unlu, M. (2010). Comparison of diagnostic performances of three different software packages in detecting coronary artery disease. *European journal of nuclear medicine and molecular imaging*, 37 (11), 2070–2078. <https://doi.org/10.1007/s00259-010-1522-1>.
  21. Slomka, P. J., Berman, D. S., Xu, Y., Kavanagh, P., Hayes, S. W., Dorbala, S., Fish, M., & Germano, G. (2012). Fully automated wall motion and thickening scoring system for myocardial perfusion SPECT: method development and validation in large population. *Journal of nuclear cardiology : official publication of the American Society of Nuclear Cardiology*, 19(2), 291–302. <https://doi.org/10.1007/s12350-011-9502-9>.
  22. Pagley, P. R., Beller, G. A., Watson, D. D., Gimple, L. W., & Ragosta, M. (1997). Improved outcome after coronary bypass surgery in patients with ischemic cardiomyopathy and residual myocardial viability. *Circulation*, 96(3), 793–800. <https://doi.org/10.1161/01.cir.96.3.793>.
  23. Dondi, M., Rodella, C., Giubbini, R., Camoni, L., Karthikeyan, G., Vitola, J. V., Einstein, A. J., Arends, B. J., Morozova, O., Pascual, T. N., Paez, D., & I-MAP investigators (2020). Inter-reader variability of SPECT MPI readings in low- and middle-income countries: Results from the IAEA-MPI Audit Project (I-MAP). *Journal of nuclear cardiology : official publication of the American Society of Nuclear Cardiology*, 27(2), 465–478. <https://doi.org/10.1007/s12350-018-1407-4>.
  24. Vajauskas D, Burneikaite G, Celutkienė J, Komiagiene R. Inter-observer variability of reporting myocardial perfusion imaging [Abstract]. In proceedings of International Conference of Integrated Medical Imaging in Cardiovascular Diseases [Internet]. IMIC: 2016 Oct 10-14; Vienna, Austria: International Atomic Energy Agency; [cited 2023 September 1]. Available from <https://conferences.iaea.org/event/100/contributions/899/contribution.pdf>.
  25. Atwood, J. E., Jensen, D., Froelicher, V., Witzum, K., Gerber, K., Gilpin, E., & Ashburn, W. (1981). Agreement in human interpretation of analog thallium myocardial perfusion images. *Circulation*, 64(3), 601–609. <https://doi.org/10.1161/01.cir.64.3.601>.
  26. Schmid, A. M., Raunig, D. L., Miller, C. G., Walovitch, R. C., Ford, R. W., O'Connor, M., Brueggewerth, G., Breuer, J., Kuney, L., & Ford, R. R. (2021). Radiologists and Clinical Trials: Part 1 The Truth About Reader Disagreements. *Therapeutic innovation & regulatory science*, 55(6), 1111–1121. <https://doi.org/10.1007/s43441-021-00316-6>.
  27. Alexiou, S., Georgoulas, P., Angelidis, G., Valotassiou, V., Tsougos, I., Psimadas, D., Lakiotis, V., Kaspri, A., Alexopoulos, D., Apostolopoulos, D., & Vassilakos, P. (2018). Myocardial perfusion and left ventricular quantitative parameters obtained using gated myocardial SPECT: Comparison of three software packages. *Journal of nuclear cardiology : official publication of the American Society of Nuclear Cardiology*, 25(3), 911–924. <https://doi.org/10.1007/s12350-016-0730-x>.
  28. Ather, S., Iqbal, F., Gulotta, J., Aljaroudi, W., Heo, J., Iskandrian, A. E., & Hage, F. G. (2014). Comparison of three commercially available softwares for measuring left ventricular perfusion and function by gated SPECT myocardial perfusion imaging. *Journal of nuclear cardiology : official publication of the American Society of Nuclear Cardiology*, 21(4), 673–681. <https://doi.org/10.1007/s12350-014-9885-5>.

## **APPENDIX A:**

### **DETAILED METHODOLOGY**

This was a retrospective cross-sectional study that included 49 adult patients with known coronary artery disease, diagnosed via coronary angiography (one or more lesions with > 50% stenosis), referred to the Philippine Heart Center Nuclear Medicine Division for viability studies using rest-redistribution thallium-201 SPECT-MPI between January 1, 2019 and December 31, 2020.

#### **Image Acquisition and Processing**

All patients included in this study underwent viability assessment using a one-day rest-redistribution thallium-201 gated SPECT-MPI protocol. Fasting was done for four hours prior to the procedure. Baseline electrocardiograph, blood pressure, and heart rate were recorded prior to the administration of 111 MBq (3 mCi) of thallium-201 via intravenous port bolus. Gated SPECT images at rest were acquired, while redistribution images were obtained after a 4-hour interval. Imaging was done using a dual-head hybrid SPECT/CT system (Discovery NM/CT 670 ES, GE Healthcare) equipped with a low-energy high resolution (LEHR) collimator. A step-and-shoot acquisition type was followed, with camera detectors configured at 90 degrees. Thirty-two projections were obtained over a 180-degree orbit (45 degrees right anterior oblique to 45 degrees left posterior oblique). Energy windows of 30% and 20% were used over the 72 keV and 167 keV photopeaks respectively, while the ECG gating was set at a 40% R-R window. A matrix of 64 x 64 x 16 was utilized to store images, with subsequent reconstruction using filtered back projection with a Butterworth filter (cut-off 0.5 cycle/cm, order = 5). Attenuation correction was applied using low-dose CT.

#### **Automated Analysis**

Automated parameters of myocardial perfusion, wall motion, and systolic thickening for each imaging study was obtained using the Quantitative Perfusion SPECT / Quantitative Gated SPECT software (QPS/QGS, Cedars-Sinai Medical Center, Los Angeles, California, USA) with the vendor-provided normal database for resting thallium. Initial summed scores (rest), delayed summed scores (redistribution), summed difference scores (SDS), summed wall motion scores (SMS), and summed thickening scores (STS) were derived from the

automated analysis.

#### **Visual Analysis**

Image interpretation was done independently by two nuclear medicine physicians of more than 10 years of experience. Both readers were initially blinded to the automated quantification measures generated by the software as well as other available work-up information. Limited clinical data, including the patient's sex, age, height, weight, and symptoms at the time of scan, were provided as these directly affected scan reading.

The American Heart Association (AHA) 17-segment model was used in image interpretation. Perfusion defects were graded with the use of a 5-point system (0 - normal; 1 - mildly decreased; 2 - moderately decreased; 3 - severely decreased; 4 - absent uptake), and from these observations, the following were derived: visual initial summed scores, delayed summed scores, and summed difference scores. Noncorrected (NC) and attenuation corrected (AC) scan images were scored separately. Visual analysis of wall motion and systolic thickening was conducted using the following grading scales: a scale of 0-5 for segmental wall motion (0 - normal; 1 - mildly hypokinetic; 2 - moderately hypokinetic; 3 - severely hypokinetic; 4 - akinetic; 5 - dyskinetic), and a scale of 0-3 for wall thickening (0 - normal; 1 - mildly reduced; 2 - moderately to severely reduced; 3 - no thickening).

## INTER-READER COMPARISON OF PERFUSION AND LV FUNCTION

TABLE B1. Inter-reader comparison of visual assessment of perfusion and LV function

	Reader 1	Reader 2	p-value
	Median (IQR)		
Visual Perfusion			
NC			
Rest SS	25 (19 to 32)	21 (12 to 29)	0.060
Redistribution SS	22 (12 to 27)	21 (11 to 27)	0.752
SDS	5 (1 to 7)	0 (0 to 1)	< 0.001
AC			
Rest SS	20 (14 to 28)	12 (7 to 21)	0.002
Redistribution SS	16 (10 to 23)	11 (6 to 20)	0.097
SDS	3 (0 to 6)	0 (0 to 1)	< 0.001
Visual + Automated Perfusion			
NC			
Rest SS	25 (17 to 32)	21 (12 to 29)	0.125
Redistribution SS	21 (12 to 27)	21 (11 to 27)	0.870
SDS	4 (2 to 6)	0 (0 to 1)	< 0.001
AC			
Rest SS	20 (13 to 27)	12 (7 to 21)	0.002
Redistribution SS	17 (10 to 23)	11 (6 to 20)	0.101
SDS	3 (0 to 6)	0 (0 to 10)	< 0.001
Visual Gated LV Function			
SMS	41 (19 to 52)	46 (29 to 53)	0.529
STS	23 (15 to 28)	30 (18 to 35)	0.061
Visual + Automated Gated			
SMS	41 (21 to 52)	46 (29 to 53)	0.614
STS	23 (15 to 29)	30 (18 to 35)	0.062



## AnyScan® TRIO Product Line SPECT, SPECT/CT and SPECT/CT/PET Molecular Imaging Scanners

Triple-NaI-Detector SPECT/CT for quantitative and high-performance 360° PET-Like imaging and workflow for diagnostic and theranostic applications.

The AnyScan® triple modality platform uniquely integrates SPECT, CT and PET for clinical NM imaging in a single scanner for dual- and triple-detector systems.



## HOLOGIC®

### Horizon™ DXA System An Innovative Solution for Accurate Diagnosis

Hologic, the pioneer in X-ray based bone densitometry, takes advanced health assessment to a new level with the Horizon DXA System. This multi-faceted system can help clinicians assess bone health, body composition and cardiovascular risk — critical elements that will help patients keep life in motion.



## RADIO PHARMA SOLUTIONS



Find your solution for your radiopharmaceutical production

Iba offers complete solutions for your radiopharmaceutical production. You can extend your tracer production for programs beyond oncology, such as cardiology and neurology.



### VDC-606 Touch Screen Dose Calibrator

- 10" touch screen medical certified PC
- Easy to use
- IBC-LITE software included
- Accurate and fast measurements
- FDA approved and Medical Device
- Available for vials and syringes
- VIK-202 or VIK-203 ionisation chamber



## EUROMEDICAL INSTRUMENTS

### Gamma and Fluorescence bi-modal detection

With a single readout module and numerous gamma probe options, the Europrobe 3.2 is a unique system that fulfills all needs of pre and post-operative detection as well as per-cutaneous localisation within 7 major clinical fields.



### Urea Breath Test Innovator

14C Urea Breath Test is used for primary diagnosis and post-treatment follow-up of H. pylori infections. The individual to be tested simply swallows 14C-urea. If H. pylori presents, the enzyme urease produced by H. pylori will metabolize 14C-urea to 14CO2 and ammonia. Then 14CO2 is transported in the blood to the lungs. When the patient exhales after a defined time this 14CO2 is captured in a breath collection card.



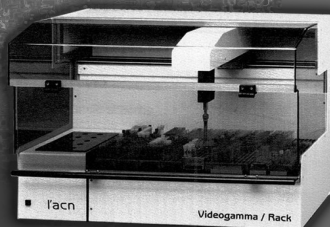
### Captus® 4000e Thyroid Uptake System

A comprehensive Nuclear Medicine Measurement System, with specific software modules for thyroid uptake, bioassay, wipe tests, automated quality assurance tests, and isotope library. Includes a fully functional 1024 channel MCA with auto and manual calibration. Timed activity mode features a programmable repetitive timed measurement program.



### Particle counter VIDEOGAMMA RACK

The first apparatus of a new generation of gamma counters. It is the first device at all that allows measurements without needing to download the tubes from their rack. It is the first instrument in the world designed for carrying automatically tubes from their rack to the detection system. For the first time the area where measurement takes place and the area where tubes are positioned are separated. In this way any kind of interference is excluded.



# A retrospective study on the concordance of the OSEM and Q.Clear reconstruction algorithms in $^{18}\text{F}$ -FDG PET-CT imaging of female patients with breast cancer

Timothy James O. Lam, MD, Sean Ira G. Gacula, MD

Department of Radiological Sciences, Section of Nuclear Medicine and PET-CT Center, Cardinal Santos Medical Center  
E-mail address: timothyjameslam@yahoo.com

## ABSTRACT

### **Objective:**

*This study examines the concordance of imaging interpretation between the Q.Clear and OSEM algorithms used in image reconstruction of PET-CT scans in female breast cancer at different stages of management.*

### **Methodology:**

*This is a retrospective cohort study of PET-CT scans of female patients with biopsy-proven breast cancer, categorized into three groups according to clinical indication. Shapiro-Wilk test was performed to verify normal distributions. SUV parameters were analyzed with paired T-test. Cohen's kappa was used to measure agreement between the two algorithms.*

### **Results:**

*PET-CT scans of 105 female breast cancer patients, aged 24-89 years, with mean BMI of  $24.9 \pm 4.5$ , referred for staging (34%), treatment evaluation (22%), and recurrence detection (44%) were included. Intraclass correlation coefficients demonstrated perfect agreement ( $k=1.0$ ) for all groups. Metabolic responses per lesion had moderate agreement ( $k=0.593$ ) with more favorable responses seen in Q.Clear for discordant lesions. Significantly higher average SNR for liver and target lesions ( $p<0.0001$  and  $p=0.0008$ , respectively) and average SUVmax and SULmax for target lesions ( $p=0.0254$  and  $p=0.0267$ , respectively) were calculated in Q.Clear. Differences for SUV and SUL parameters of reference regions were not statistically significant.*

### **Conclusion:**

*Q.Clear and OSEM algorithms were concordant for staging, treatment evaluation, and recurrence detection in PET-CT scans of female breast cancer patients. Q.Clear may be used preferably for its higher SNR. However, we recommend using the same PET-CT reconstruction algorithm for treatment evaluation due to significant differences in SUVmax and SULmax for target lesions between the two algorithms.*

**Keywords:** Q.Clear, PET-CT, reconstruction algorithm, breast cancer

## INTRODUCTION

As of 2020, female breast cancer has surpassed lung cancer as the leading cause of cancer incidence worldwide. It ranks 5th globally and ranks 1st in 110 countries in cancer-related mortality, accounting for one in six cancer deaths [1]. The management of breast cancer involves a multidisciplinary approach with nuclear medicine and molecular imaging techniques, particularly positron emission tomography -

computed tomography (PET-CT) using fluorine-18 fluorodeoxyglucose ( $^{18}\text{F}$ -FDG), playing an important role [2]. At the PET-CT center of our institution, breast cancer is second only to lung cancer as the most common cause for referral. Although functional imaging with  $^{18}\text{F}$ -FDG PET-CT is not routinely used in breast cancer upon diagnosis, it is accepted in the staging of many cancers [3]. Staging of breast cancer is performed to stratify patients into risk categories that define prognosis and guide treatment recommendations [4]. There are studies that show PET-CT is better than CT alone for

for detecting small tumors, nodal and distant metastases, and for monitoring treatment response in breast cancer patients [5][6].

The current standard for PET-CT imaging reconstruction is the use of the ordered subset expectation maximization (OSEM), an iterative statistical algorithm [7]. Because of increasing background noise with each iteration, a disadvantage of using this algorithm is that it is terminated early, preventing it from reaching full convergence of 25 iterations which suffers from high noise [8][9]. In the clinical setting, most PET centers use CT attenuation corrected (AC) images reconstructed with two to five iterations [10]. Innovatively, a relatively new Bayesian penalized-likelihood (BPL) iterative PET reconstruction algorithm developed by GE Healthcare, called Q.Clear, has been introduced into GE PET-CT scanners. This algorithm can control background noise in image reconstructions with full convergence, increasing the signal-to-noise ratio (SNR), thus improving image quality. Q.Clear has been described as a fully convergent PET image reconstruction technique designed to provide excellent image quality and consistent and accurate quantitation [9].

To date, there is still limited data on the use of Q.Clear in the clinical setting. Several studies have been published on its application in certain malignancies, including lung cancer with or without metastasis [11][12][13], metastatic colorectal cancer [14], and lymphoma [15][16]. Although these studies have reported the clear advantages of this algorithm, its application in clinical practice is still left generally undecided and warrants further investigation.

## OBJECTIVE

This study aims to examine the concordance of the Q.Clear algorithm with the standard OSEM algorithm in the interpretation of PET-CT imaging in female breast cancer patients at different stages of management: (1) upon diagnosis for initial staging prior to commencement of treatment, (2) evaluation of response to treatment, and (3) detection of disease recurrence. With the recent rise of female breast cancer as the most commonly diagnosed form of malignancy, it is imperative that further advancement in our approach to this disease through clinical research parallel its escalation. .

## METHODOLOGY

### Materials

A total of 4,460 18F-FDG PET-CT scans were performed  
Phil J Nucl Med 2025; 20(1): 50 - 59

between March 2017 to May 2021. Out of 639 PET-CT scans of adult, female patients with histopathologically proven invasive mammary carcinoma, 105 eligible scans were included in this study. Scans of patients with multiple primary malignancies, incomplete or irretrievable images, and incomplete clinical records were excluded. As analysis of reference regions require physiologic 18F-FDG distribution in the liver, patients with extensive hepatic metastasis precluding proper physiologic liver SUV determination were likewise excluded. Scans were categorized to one of three groups according to clinical indication: staging prior to initiation of treatment (S-PET), evaluation of response to interim or completed treatment (T-PET), and surveillance for the detection disease recurrence (R-PET).

### Machine and equipment

A single GE Discovery 710 model PET-CT scanner was used with gantry bore diameter of 70 cm and a spatial resolution of approximately 4.5 mm. The PET system is able to collect data in 3D mode and can reconstruct both the standard OSEM and Q.Clear images with or without time-of-flight (TOF) and point-spread function modeling (SharpIR). A CT injection system was used for all contrast administration. Visual evaluation and semi-quantitative measurement of standard uptake values (SUV) was performed using a GE advantage workstation version 4.7 which provides maximum intensity projections (MIPs), multi-slice PET and CT images, and their fusion.

### Imaging procedure and technique

Patients underwent at least six hours of fasting before the examination. Blood glucose levels were evaluated prior to IV administration of F-18 FDG with an acceptable limit of less than 200 mg/dl. Image acquisition was obtained 60 ± 10 minutes after the injection of 0.12 mCi/kg body weight 18F-FDG. Whole body scans covered the head to the either the mid-thigh or the feet with 8 ± 1 or 14 ± 1 bed positions, respectively. For scans from head to mid-thigh, the acquisition time was 120 seconds per bed position. For scans from head to feet, acquisition time was 90 seconds per bed position from head to mid-thigh and 60 seconds per bed position from mid-thigh to feet. PET images were reconstructed with both OSEM and Q.Clear algorithms. OSEM reconstruction was performed with a 70-cm dual field of view (DFOV) into a 192 × 192 matrix with 3 iterations and 24 subsets. Reconstruction with Q.Clear was performed with penalization (β) factor of either 400 or 500.

### Imaging evaluation

All included PET-CT scans were evaluated and interpreted separately by two nuclear medicine

physicians (NMPs) from a pool of five NMP staff with at least two to five years of experience. Evaluating NMPs are either diplomates or fellows of the Philippine Society of Nuclear Medicine (PSNM) who had fellowship training in PET-CT interpretation from the University of Zurich in Switzerland. In cases of equivocal interpretations, the diagnostic conclusion was made by a consensus between the evaluating NMPs. Diagnostic conclusions were made according to the indication for referral and were grouped as follows:

- S-PET: Cancer was staged according to the 8th edition of the TNM staging system developed and maintained by American Joint Committee on Cancer (AJCC) [17].
- T-PET: Evaluation of overall treatment response was based on the European Organization for Research and Treatment of Cancer (EORTC) PET response criteria [18]. Metabolic responses of individual target lesions, likewise, derived from the EORTC PET response criteria, are defined in Table 1.
- R-PET: Interpretation of scan were classified as to having evidence of disease recurrence (positive) or no detectable disease (negative).

**TABLE 1.** Metabolic response evaluation of target lesion

Response category	Criteria
Complete response	Resolution of FDG uptake
Partial response	> 25% decrease in SUV <sub>max</sub>
Metabolically stable	< 25% change in SUV <sub>max</sub>
Metabolic progression	> 25% increase in SUV <sub>max</sub>
Based on the EORTC PET response criteria (1999)	

### Semi-quantitative measurements for reference regions and target lesions.

The parameters (e.g., maximum, mean, peak, standard deviation) of the standard uptake value (SUV) and its correction for lean body mass (SUL) were recorded using a standard volume of interest (VOI) tool. Reference regions were measured with 3.0 cm diameter spherical VOIs both in the right lobe of liver and descending aorta (at the level immediately below the aortic arch) representing the mediastinal blood pool (MBP). The primary or metastatic lesion with the highest SUV<sub>max</sub> was designated as the “target lesion”. For scans with the intent of evaluating treatment response (T-PET), the target lesion is chosen based on the prior PET-CT images

for comparison. Signal-to-background ratio (SBR) for each target lesion was calculated as the maximum value of the target lesion VOI (SUV<sub>max</sub> or SUL<sub>max</sub>) divided by mean value of the liver VOI (SUV<sub>mean</sub> or SUL<sub>mean</sub>). Signal-to-noise ratio (SNR) for target lesions was calculated as maximum value of the target lesion VOI (SUV<sub>max</sub> or SUL<sub>max</sub>) divided by standard deviation of the liver VOI (SUV<sub>sd</sub> or SUL<sub>sd</sub>), while SNR for the liver was calculated as mean value of the liver (SUV<sub>mean</sub> or SUL<sub>mean</sub>) divided by the standard deviation of the liver (SUV<sub>sd</sub> or SUL<sub>sd</sub>). The standard deviation value of the liver VOI was used as a measure of noise for this study.

### Statistical analysis.

The OpenEpi version 3.01, Epi Info version 7.2, and SPSS statistics 20 were used for statistical analysis. The Shapiro-Wilk test was performed to verify normal distributions. Paired T-test was used to determine the mean difference of SUV and SUL parameters between the Q.Clear and OSEM reconstruction algorithms, for reference regions in the liver and MBP and identifiable target lesions across the entire cohort. The p-value generated from the statistical calculator determined the significance level of each group. A p-value of less than 0.05 was considered statistically significant. Cohen's kappa (k) was used to calculate the intraclass correlation coefficient between the two algorithms for the three groups.

### Ethics approval and consent

This study was conducted in strict compliance with the provisions provided in the Philippine Data Privacy Act of 2012 (Republic Act No. 10173). All imaging procedures performed were in accordance with the rules and principles of the 1964 Declaration of Helsinki, including its subsequent amendments. Through the Research Ethics Review Committee of our institution, a waiver for informed consent was granted given its retrospective approach.

## RESULTS

### Clinical characteristics

A total of 105 scans were included and retrospectively analyzed, of which 36 scans were assigned in the S-PET group, 23 in the T-PET group, and 46 in the R-PET group. Patients were of Asian (Chinese or Filipino) descent. Sixty-three patients (60%) were above the upper limit of normal BMI for Asians ( $\geq 23$ ). (See Table 2).

**TABLE 2.** Patients characteristics per group

Group	S-PET (n=36)	T-PET (n=23)	R-PET (n=46)	Total (n=105)
Age (years)				
Range	24-89	36-75	32-83	24-89
Median	61	58	58.5	60
Mean	59 ± 14.5	56.7 ± 13.6	57.8 ± 11.9	57.9 ± 13.1
Weight (kg)				
Range	38-99	44-114	44-96	38-114
Median	57	57	58	57
Mean	60.8 ± 14.4	59.4 ± 14.3	60.8 ± 10.5	60.4 ± 12.7
BMI (kg/m <sup>2</sup> )				
Range	17.8-40.2	17.2-39.4	19.0-34.0	17.2-40.2
Median	24.8	23.0	24.8	24.7
Mean	25.4 ± 5.1	24.1 ± 4.6	24.9 ± 4.0	24.9 ± 4.5

Abbreviations: BMI Body mass index

**TABLE 4.** Staging of disease for S-PET

Stage	OSEM				
	I	II	III	IV	Total
I	6	0	0	0	6
II	0	9	0	0	9
III	0	0	5	0	5
IV	0	0	0	16	16
Total	6	9	5	16	36

Symmetric Measures				
Value	Asymp. Std. Error <sup>a</sup>	Approx. T <sup>b</sup>	Approx. Sig	
Measurement of agreement <i>k</i>	1.000	<0.001	9.800	<0.001
N of valid cases	36			

a. Not assuming the null hypothesis.

b. Using the asymptotic standard error assuming the null hypothesis.

**TABLE 3.** Summary of background SUV and SUL parameter analysis for reference regions across the entire cohort (n = 105)

	OSEM Mean ± SD (range)	Q.Clear Mean ± SD (range)	Mean diff. (95% CI)	<i>p</i> value
SUV parameters				
Aorta SUV <sub>max</sub>	2.86 ± 0.64 (1.21-4.82)	2.76 ± 0.60 (1.45-4.45)	-0.10 (-0.27 to 0.07)	0.2511
Aorta SUV <sub>mean</sub>	2.03 ± 0.49 (0.61-3.28)	2.06 ± 0.46 (0.72-3.24)	0.03 (-0.10 to 0.16)	0.6049
Aorta SUV <sub>peak</sub>	2.20 ± 0.51 (0.87-3.59)	2.20 ± 0.51 (0.75-3.44)	-0.01 (-0.14 to 0.13)	0.9476
Aorta SUV <sub>sd</sub>	0.22 ± 0.05 (0.12-0.37)	0.20 ± 0.05 (0.02-0.36)	-0.03 (-0.04 to -0.01)	<0.001
Liver SUV <sub>max</sub>	3.64 ± 0.86 (0.34-5.52)	3.48 ± 0.74 (1.70-5.00)	-0.16 (-0.38 to 0.06)	0.1460
Liver SUV <sub>mean</sub>	2.76 ± 0.60 (1.01-4.29)	2.72 ± 0.59 (0.94-3.92)	-0.04 (-0.20 to 0.12)	0.6444
Liver SUV <sub>peak</sub>	2.95 ± 0.65 (0.89-4.68)	2.87 ± 0.62 (0.90-4.6)	-0.08 (-0.25 to 0.09)	0.0794
Liver SUV <sub>sd</sub>	0.24 ± 0.08 (0.10-0.60)	0.18 ± 0.05 (0.07-0.35)	-0.05 (-0.07 to -0.03)	<0.001
Liver SUV SNR	12.52 ± 3.60 (4.01-21.25)	15.36 ± 4.03 (6.71-26.13)	2.84 (1.80 to 3.88)	<0.001
SUL parameters				
Aorta SUL <sub>max</sub>	1.97 ± 0.36 (0.76-3.09)	1.89 ± 0.46 (0.16-2.95)	-0.09 (-0.21 to 0.03)	0.1310
Aorta SUL <sub>mean</sub>	1.40 ± 0.30 (0.39-2.03)	1.44 ± 0.31 (0.46-2.52)	0.04 (-0.05 to 0.12)	0.4060
Aorta SUL <sub>peak</sub>	1.52 ± 0.31 (0.55-2.15)	1.53 ± 0.33 (0.48-2.85)	0.01 (-0.08 to 0.10)	0.8325
Aorta SUL <sub>sd</sub>	0.15 ± 0.03 (0.08-0.24)	0.14 ± 0.03 (0.08-0.30)	-0.01 (-0.02 to -0.006)	0.0014
Liver SUL <sub>max</sub>	2.56 ± 0.50 (0.95-3.66)	2.40 ± 0.46 (1.08-3.58)	-0.16 (-0.29 to -0.02)	0.0205
Liver SUL <sub>mean</sub>	1.91 ± 0.37 (0.64-2.68)	1.89 ± 0.36 (0.59-2.62)	-0.02 (-0.12 to 0.08)	0.6550
Liver SUL <sub>peak</sub>	2.04 ± 0.39 (0.57-2.69)	1.99 ± 0.37 (0.57-2.69)	-0.06 (-0.16 to 0.05)	0.2743
Liver SUL <sub>sd</sub>	0.16 ± 0.06 (0.08-0.60)	0.13 ± 0.03 (0.05-0.24)	-0.04 (-0.05 to -0.02)	<0.001
Liver SUL SNR	12.50 ± 3.54 (2.55-20.60)	15.45 ± 4.07 (6.55-27.75)	2.95 (1.91 to 3.98)	<0.001

Note: The liver SUV<sub>sd</sub> was used as the measure for noise

## Reference regions

Analysis for reference regions included the entire cohort (n=105). For the MBP, there was no statistically significant difference for all SUV and SUL parameters between Q.Clear and OSEM. For the liver, differences in SULmean, SULpeak, and all SUV parameters were likewise not statistically significant. The average liver SULmax was significantly lower with Q.Clear (*p* = 0.0205),

albeit a small mean diff. of -0.16 (95% CI -0.29 to -0.02). The standard deviation of the liver VOI was significantly lower for both SUV and SUL parameters (*p* < 0.001) with Q.Clear. Accordingly, average SNR for the liver was significantly higher (*p*<0.001) for both SUV and SUL in Q.Clear with a mean diff. of 2.84 (95% CL 1.80 to 3.88) and 2.95 (95% CI 1.91 to 3.98), respectively. (See Table 3).

## Target lesions

Across the entire cohort, 48 identifiable target lesions within normal distribution were included in the final analysis. The average SUV<sub>max</sub> and SUL<sub>max</sub> were significantly higher ( $p = 0.0254$  and  $p = 0.0267$ , respectively) with Q.Clear than OSEM with a mean diff. of 1.27 (95% CI 0.16 to 2.38) and 0.93 (95% CI 0.11 to 1.76), respectively. The average Q.Clear-to-OSEM uptake ratio was 1.23 for SUV<sub>max</sub> and 1.25 for SUL<sub>max</sub>, with an average percent change (%Δ) of 23%. There was no statistically significant difference for SUV<sub>peak</sub> and SUL<sub>peak</sub>. The average SNR of the target lesions were significantly higher ( $p < 0.001$ ) for both SUV and SUL with mean diff. of 14.25 (95% CI 6.05 to 22.44) and 13.96 (95% CI 5.90 to 22.02), respectively. Signal-to-background ratio was significantly higher ( $p = 0.0473$ ) when using SUV with a mean diff. of 0.66 (95% CI 0.008 to 1.32), while no statistically significant difference was noted when using SUL. (See Table 5).

## Staging of disease

Patients in the S-PET group were referred for pre-treatment staging. All 36 cases of the S-PET group demonstrated complete agreement between the Q.Clear and OSEM for all stages ( $k = 1.0$ ,  $p < 0.001$ ). Six cases (17%) were stage I, nine (25%) were stage II, five (13%) were stage III, and 16 (44%) were stage IV. (See Table 4).

## Metabolic responses of individual target lesions and overall treatment response.

Patients in the T-PET group were referred for either interim or end of treatment response evaluation.

Eighteen patients (78.3%) underwent surgery (i.e., simple mastectomy or modified radical mastectomy), eight (34.8%) had radiotherapy, and all underwent a form of antineoplastic drug treatment (e.g., chemotherapy, immunotherapy, targeted, or hormonal therapy). Concordance of metabolic responses were analyzed for all identifiable target lesions in the T-PET group ( $n = 23$ ) based on semi-quantitative measurements. Similar metabolic responses were observed between the two algorithms in 16 cases (69%) with concordance analysis showing moderate agreement ( $k = 0.593$ ,  $p < 0.001$ ). There were seven (30%) discordant per-lesion metabolic responses. Among these, five out of seven (71%) showed more favorable responses with Q.Clear. (See Table 6).

Despite these discrepancies in metabolic responses on a per-lesion basis, the diagnostic conclusion for overall treatment response per patient was concordant in all 23 cases ( $k = 1.0$ ,  $p < 0.001$ ). Two cases (8%) had complete metabolic response, seven cases (30%) had partial metabolic response, two cases (8%) had stable metabolic disease, and 12 cases (52%) had progressive metabolic disease. (See Table 7).

## Detection of disease recurrence

All 46 cases of the R-PET group also showed full agreement between the Q.Clear and OSEM algorithms ( $k = 1.0$ ,  $p < 0.001$ ). Twenty-two (48%) cases had evidence of disease recurrence while 24 (52%) had no detectable disease. (See Table 8).

**TABLE 5.** Summary of included target lesions analysis ( $n = 48$ )

	OSEM Mean $\pm$ SD (range)	Q.Clear Mean $\pm$ SD (range)	Mean diff. (95% CI)	$p$ value	Q.Clear-to-OSEM uptake ratio
SUV parameters					
Target lesion SUV <sub>max</sub>	5.43 $\pm$ 1.98 (1.17-9.10)	6.69 $\pm$ 3.32 (1.59-18.97)	1.27 (0.16 to 2.38)	0.0254	1.23
Target lesion SUV <sub>peak</sub>	3.88 $\pm$ 1.56 (0.78-7.17)	3.88 $\pm$ 1.56 (0.78-7.17)	0.13 (-0.54 to 0.81)	0.6899	1.03
Target lesion SUV SNR	26.10 $\pm$ 13.43 (6.19-75.83)	40.34 $\pm$ 25.25 (9.36-110.67)	14.25 (6.05 to 22.44)	<0.001	
Target lesion SUV SBR	2.16 $\pm$ 1.13 (0.87-6.79)	2.82 $\pm$ 1.99 (1.08-9.86)	0.66 (0.008 to 1.32)	0.0473	
SUL parameters					
Target lesion SUL <sub>max</sub>	3.76 $\pm$ 1.40 (0.74-1.93)	4.69 $\pm$ 2.51 (1.01-14.2)	0.93 (0.11 to 1.76)	0.0267	1.25
Target lesion SUL <sub>peak</sub>	2.81 $\pm$ 1.09 (0.50-2.53)	2.81 $\pm$ 1.28 (0.54-5.91)	0.12 (-0.36 to 0.61)	0.6077	1.05
Target lesion SUL SNR	25.70 $\pm$ 13.12 (6.22-65.12)	39.67 $\pm$ 24.89 (9.44-106.67)	13.96 (5.90 to 22.02)	<0.001	
Target lesion SUL SBR	2.12 $\pm$ 1.09 (0.88-6.82)	2.71 $\pm$ 1.73 (0.99-8.42)	0.58 (-0.001 to 1.17)	0.0506	

Note: The Q.Clear-to-OSEM uptake ratios were calculated by dividing the means of Q.Clear SUV parameters by OSEM SUV parameters.

**TABLE 6.** Metabolic responses of target lesions for T-PET

		OSEM				Total
		CR	PR	MS	MP	
Q.Clear	Complete response	5	0	0	0	5
	Partial response	0	5	3	0	8
	Metabolically stable	0	1	2	2	5
	Metabolic progression	0	0	1	4	5
	Total	5	6	6	6	23

Symmetric Measures				
	Value	Asymp. Std. Error <sup>a</sup>	Approx. T <sup>b</sup>	Approx. Sig.
Measurement of agreement	<i>k</i> 0.593	0.128	4.959	<0.001
N of valid cases	23			

a. Not assuming the null hypothesis.  
b. Using the asymptotic standard error assuming the null hypothesis.

**TABLE 7.** Staging of disease for S-PET

		OSEM				Total
		CR	PR	MS	MP	
Q.Clear	Complete response	2	0	0	0	2
	Partial response	0	7	0	0	7
	Metabolically stable	0	0	2	0	2
	Metabolic progression	0	0	0	12	12
	Total	2	7	2	12	23

Symmetric Measures				
	Value	Asymp. Std. Error <sup>a</sup>	Approx. T <sup>b</sup>	Approx. Sig.
Measurement of agreement	<i>k</i> 1.000	<0.001	6.984	<0.001
N of valid cases	23			

a. Not assuming the null hypothesis.  
b. Using the asymptotic standard error assuming the null hypothesis.

**TABLE 8.** Detection of disease recurrence for R-PET

		OSEM		
		Positive	Negative	Total
Q.Clear	Positive	21	0	21
	Negative	0	25	25
	Total	21	25	46

Symmetric Measures				
	Value	Asymp. Std. Error <sup>a</sup>	Approx. T <sup>b</sup>	Approx. Sig.
Measurement of agreement	<i>k</i> 1.000	<0.001	6.984	<0.001
N of valid cases	46			

a. Not assuming the null hypothesis.  
b. Using the asymptotic standard error assuming the null hypothesis.

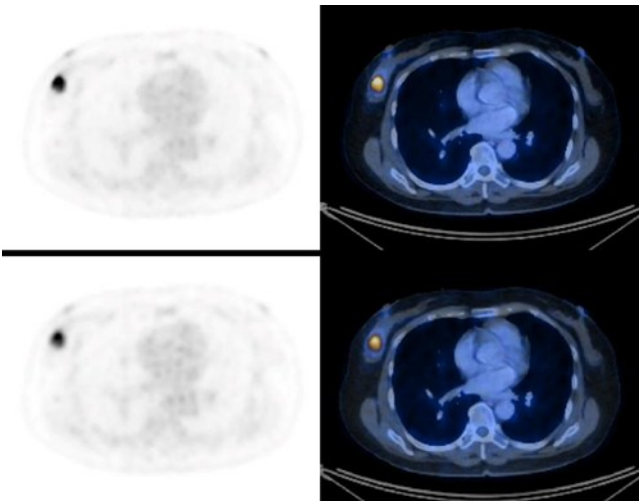


**FIGURE 1.** Q.Clear images (upper row) showing a more defined and intense uptake in the primary tumor (arrow) than with OSEM (lower row) with similar visual level of background noise and mediastinal activity.

## DISCUSSION

Compared to the widely used OSEM reconstruction algorithm, BPL image reconstruction algorithms have the unique advantage of reaching full convergence with similar visual noise properties by using the relative difference penalty. It aims to improve accuracy of quantitative measurements without compromising visual image quality [19][20][21] The BPL algorithm Q.Clear has been found to improve image quality, with higher recovery coefficients and lower background variability [22]. Since most PET imaging evaluation criteria are based upon the use of the standard OSEM algorithm, the application of Q.Clear, with its potential to modify

Phil J Nucl Med 2025; 20(1): 50 - 59

imaging interpretation, warrants investigation into its conformity with these existing criteria.

Semi-quantitative measurements using SUV in the evaluation of lesions has its limitations but are partly resolved when lesion SUVs are normalized to reference region SUVs [23]. Therefore, inter-algorithm variability of reference region activity should not be substantially divergent to maintain concordance of the significance of lesional uptake. The difference of VOI reference regions in the MBP and liver between the two algorithms were not statistically significant in our study. Average SUV and SUL parameters were mostly lower with Q.Clear than OSEM, similar to Wyrzykowski et al. who likewise had

slight decrease in the SUVmax of reference regions [15]. This is in contrast to the findings of Teoh et al. [11][12] and Parvizi et al. [14] whom had significantly higher average MBP and liver SUV parameters with the BPL algorithm. A  $\beta$  factor of 400 was used by the former, 500 by the latter, and either 400 or 500 for our scans. For both authors, commencement of imaging was done after 90 minutes, and acquisition time was 2x longer than ours. We presume that since similar  $\beta$  factors were used among the studies, the timing of imaging commencement and acquisition time may have been the reason for the diametric semi-quantitative results for the reference regions. In any case, reference regions in our study did not vary significantly between the two algorithms. Among the SUV parameters, SUVmean of the liver has been found to be the most stable or least variable over different acquisition times [24] while the SULmean of the liver had excellent inter-reader agreement with similar values and variance irrespective of VOI placement within the right lobe of the liver [25].

One aspect we considered for different reconstruction algorithms to be concordant is the visual similarity of images to the clinical eye of the evaluating physician. Quality of images being evaluated may influence scan interpretation and is usually reflected by the level of noise in the background. As seen in our results, the SNR for the liver and target lesions was significantly higher with Q.Clear. Similarly, in addition to the aforementioned studies, a study by Chilcott et al. comparing the two algorithms over a range of patient weights likewise showed a significantly higher liver SNR using BPL compared to OSEM for all BMI groups [26]. Interestingly, their study also showed that OSEM had increasing noise with increasing weight and BMI whereas BPL had no significant change. In agreement, a study by Vallot et al. concluded that BPL is especially appropriate for patients with a high BMI as it improves the SNR for all uptakes [27]. Although SUV ratios used to measure response to treatment are less dependent on noise [28], the resultant higher SNR, and consequently better image quality, may be beneficial in detecting subtle changes in lesions visually since image feature differences (e.g. shape, intensity, and gray-level co-occurrence matrix) in PET scans increases as the noise level increases [29]. (See Figure 1).

With the increasing number of iterations in PET image reconstruction, the SUV parameters would presumably increase, as is with noise, resulting to discordant SUV measurements between OSEM and BPL algorithms.

Opposingly, Q.Clear demonstrated lower noise and reference region SUVs. Similarly with the studies of Wyrzykowski, Teoh, and Parvizi, the average SUVmax for target lesions were significantly higher with Q.Clear in our study as is with SULmax. The average  $\% \Delta$  of 23% for both SUV and SUL maximum uptake values was akin to Teoh who had a  $\% \Delta$ SUVmax of 23.7% for histopathologically positive nodules ( $n = 25$ ). A lower increment was seen in nodules negative for metastasis in their study. Lesions that were deemed non-malignant or inflammatory in nature were not analyzed in our study even if their SUVmax was higher than included target lesions. Interestingly, not all target lesions in our study showed increases in uptake with Q.Clear and as much as eight (16%) lesions exhibited decreases in SUVmax. The difference in SUV and SUL peak values between the two algorithms was not statistically significant as opposed to Parvizi who had significantly higher SUVpeak for lesions ( $n = 45$ ) with the BPL algorithm. Although SUVmax is presently the most widely used parameter for semi-quantitative measurements of lesions, SUVpeak has been proposed as a stronger alternative [30] and may increase the reproducibility and accuracy of quantitative PET studies necessary for treatment response evaluation [24]. But further research into its application would be needed for it to be considered a potential alternative to the more extensively employed SUVmax.

It is crucial for preliminary staging of breast cancer to be precise as possible as it may consequently affect initial and long-term treatment. Imaging plays a very important role in the evaluation of metastasis and the utility of PET-CT scans can lead to the upstaging or downstaging of breast cancer [31][32]. Ideally, stage of disease evaluated using an alternative PET reconstruction algorithm should not deviate from the standard OSEM, as contradicting disease extent may lead to unwarranted confusion in management. Our study showed complete concordance in breast cancer staging between the two algorithms. The importance of this agreement is further supported by evidence of PET/CT significantly contributing to the accurate staging and management of breast cancer, starting from stage IIA [33]. Coincidentally, the majority of patients (83%) in the S-PET group were stage II and above.

Overall treatment response was concordant for all cases in the T-PET group in the context that diagnostic conclusions were made considering responses not solely based on the target lesion but including all other lesions in its entirety. Hence, the discordant but more favorable

semi-quantitative metabolic responses seen in single target lesions with Q.Clear, did not reflect in this outcome. This signifies one important value of PET/CT in identifying evidence of heterogeneous metabolic responses of different metastatic lesions [34]. Additionally, this may potentially aid in avoiding unnecessary and costly treatment escalation in cases of solitary lesions on follow-up. Although studies have been published on the utility of PET in solitary lesions in the lung [35][36][37] and liver [38], these are mainly exploring its value in determining probability for malignancy and not for treatment response as in this case.

Several studies have already been published on the benefit of using 18F-FDG PET-CT for the diagnosis of disease recurrence in breast cancer [39][40][41]. The study of Radan et al. found that the use of PET-CT imaging led to changes in the subsequent clinical management in as much as 51% of breast cancer patients [39]. Our study showed complete concordance of scans, both in positive and negative cases of recurrence between the two algorithms. We found that lesions likely ascribed to disease recurrence can be reliably detected in both the Q.Clear and OSEM algorithms by our experienced NMPs. In our anecdotal observations, the evaluating NMPs expressed a greater degree of confidence with PET-positive lesions seen in Q.Clear reconstructed images as they had higher uptake values and were more visually striking albeit these same lesions were similarly regarded as positive for recurrence on OSEM. Agreeingly, the study of Sampaio et al. concluded that Q.Clear can impact on NMPs' reading confidence and accuracy by improving image quality and quantitation capacity [42]. (See Figure 2).

### Limitations of this study

The differences in acquisition time between the head-to-mid thigh scans and head-to-feet scans resulted in a 30-second disparity between the two ranges of imaging which may have affected SUV quantification. The shorter acquisition time stemmed from the need to improve logistics for patient scheduling to adjust for the more comprehensive head-to-feet scans. The small sample size for target lesions included in the final analysis was a result of excluding outliers in the data to achieve normal distribution.

## CONCLUSION

The Q.Clear reconstruction algorithm was concordant with the



**FIGURE 2.** Small focus of increased FDG activity better visualized in the Q.Clear image (right) with similar background activity in the surrounding structures. Although this was regarded as non-specific and did not affect the final diagnostic conclusion.

standard OSEM for PET-CT imaging interpretation in female breast cancer patients for staging, evaluation of treatment response, and detection of disease recurrence. It is an alternative algorithm that may be used preferably, given its higher SNR for both liver and target lesions. However, despite concordance in diagnostic conclusions, we recommend using the same PET-CT reconstruction algorithm on follow-up in comparing studies for treatment response evaluation due to the significant differences in average SUVmax and SULmax for target lesions between the two algorithms.

### Disclosure

The authors declare no conflicts of interest relevant to the conduction and authorship of this study.

### Acknowledgement

The authors express their utmost gratitude to Ms. Ma. Kristine Joy S. Calvario and Dr. Candice Genuino-Montañó for their guidance in the construction of the protocol up to finalization of the manuscript.

## REFERENCES

1. Sung, H., Ferlay, J., Siegel, R. L., Laversanne, M., Soerjomataram, I., Jemal, A., & Bray, F. (2021). Global Cancer Statistics 2020: GLOBOCAN Estimates of Incidence and Mortality Worldwide for 36 Cancers in 185 Countries. *CA: a cancer journal for clinicians*, 71(3), 209–249. <https://doi.org/10.3322/caac.21660>
2. Yazarbas, U., Avci, N. C., Yeniay, L., & Argon, A. M. (2018). The value of 18F-FDG PET/CT imaging in breast cancer staging. *Bosnian journal of basic medical sciences*, 18(1), 72–79. <https://doi.org/10.17305/bjbms.2017.2179>
3. Turner, N. C., & Jones, A. L. (2008). Management of breast cancer--part I. *BMJ (Clinical research ed.)*, 337(7661), a421. <https://doi.org/10.1136/bmj.a421>
4. Menon, G., Alkabban, F. M., & Ferguson, T. (2024). Breast Cancer. In *StatPearls*. StatPearls Publishing

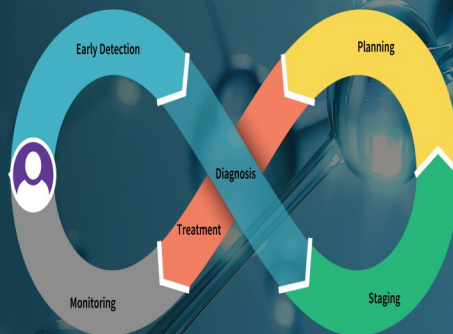
5. Yang, S. K., Cho, N., & Moon, W. K. (2007). The role of PET/CT for evaluating breast cancer. *Korean journal of radiology*, 8(5), 429–437. <https://doi.org/10.3348/kjr.2007.8.5.429>
6. Shawky, M., Ali, Z.A.E., Hashem, D.H. et al. 2020. Role of positron-emission tomography/computed tomography (PET/CT) in breast cancer. *Egypt J Radiol Nucl Med* 51, 125 (2020). <https://doi.org/10.1186/s43055-020-00244-9>.
7. Lantos, J., Mittra, E. S., Levin, C. S., & Iagaru, A. (2018). Standard OSEM vs. regularized PET image reconstruction: qualitative and quantitative comparison using phantom data and various clinical radiopharmaceuticals. *American journal of nuclear medicine and molecular imaging*, 8(2), 110–118.
8. Tong, S., Alessio, A. M., & Kinahan, P. E. (2010). Image reconstruction for PET/CT scanners: past achievements and future challenges. *Imaging in medicine*, 2(5), 529–545. <https://doi.org/10.2217/iim.10.49>.
9. Ross S. Q.Clear (GE Healthcare White Paper). [http://www3.gehealthcare.co.uk/~media/documents/us-global/products/petct/whitepaper/q%20clear/ge-healthcare-white-paper\\_qclear.pdf](http://www3.gehealthcare.co.uk/~media/documents/us-global/products/petct/whitepaper/q%20clear/ge-healthcare-white-paper_qclear.pdf). 2015.
10. Jaskowiak, C. J., Bianco, J. A., Perlman, S. B., & Fine, J. P. (2005). Influence of reconstruction iterations on 18F-FDG PET/CT standardized uptake values. *Journal of nuclear medicine : official publication, Society of Nuclear Medicine*, 46(3), 424–428.
11. Teoh, E. J., McGowan, D. R., Bradley, K. M., Belcher, E., Black, E., & Gleeson, F. V. (2016). Novel penalised likelihood reconstruction of PET in the assessment of histologically verified small pulmonary nodules. *European radiology*, 26(2), 576–584. <https://doi.org/10.1007/s00330-015-3832-y>.
12. Teoh, E. J., McGowan, D. R., Bradley, K. M., Belcher, E., Black, E., Moore, A., Sykes, A., & Gleeson, F. V. (2016). 18F-FDG PET/CT assessment of histopathologically confirmed mediastinal lymph nodes in non-small cell lung cancer using a penalised likelihood reconstruction. *European radiology*, 26(11), 4098–4106. <https://doi.org/10.1007/s00330-016-4253-2>.
13. Messerli, M., Stolzmann, P., Egger-Sigg, M., Trinckauf, J., D'Aguzzo, S., Burger, I. A., von Schulthess, G. K., Kaufmann, P. A., & Huellner, M. W. (2018). Impact of a Bayesian penalized likelihood reconstruction algorithm on image quality in novel digital PET/CT: clinical implications for the assessment of lung tumors. *EJNMMI physics*, 5(1), 27. <https://doi.org/10.1186/s40658-018-0223-x>.
14. Parvizi, N., Franklin, J. M., McGowan, D. R., Teoh, E. J., Bradley, K. M., & Gleeson, F. V. (2015). Does a novel penalized likelihood reconstruction of 18F-FDG PET-CT improve signal-to-background in colorectal liver metastases?. *European journal of radiology*, 84(10), 1873–1878. <https://doi.org/10.1016/j.ejrad.2015.06.025>.
15. Wyrzykowski, M., Siminiak, N., Kaźmierczak, M., Ruchała, M., & Czepczyński, R. (2020). Impact of the Q.Clear reconstruction algorithm on the interpretation of PET/CT images in patients with lymphoma. *EJNMMI research*, 10 (1), 99. <https://doi.org/10.1186/s13550-020-00690-6>.
16. Ly, J., Minarik, D., Edenbrandt, L., Wollmer, P., & Trägårdh, E. (2019). The use of a proposed updated EARL harmonization of 18F-FDG PET-CT in patients with lymphoma yields significant differences in Deauville score compared with current EARL recommendations. *EJNMMI research*, 9(1), 65. <https://doi.org/10.1186/s13550-019-0536-3>.
17. Kalli, S., Semine, A., Cohen, S., Naber, S. P., Makim, S. S., & Bahl, M. (2018). American Joint Committee on Cancer's Staging System for Breast Cancer, Eighth Edition: What the Radiologist Needs to Know. *Radiographics : a review publication of the Radiological Society of North America, Inc*, 38(7), 1921–1933. <https://doi.org/10.1148/rg.2018180056>.
18. Lasnon, C., Quak, E., Le Roux, P. Y., Robin, P., Hofman, M. S., Bourhis, D., Callahan, J., Binns, D. S., Desmonts, C., Salaun, P. Y., Hicks, R. J., & Aide, N. (2017). EORTC PET response criteria are more influenced by reconstruction inconsistencies than PERCIST but both benefit from the EARL harmonization program. *EJNMMI physics*, 4(1), 17. <https://doi.org/10.1186/s40658-017-0185-4>.
19. Ahn, S., Ross, S. G., Asma, E., Miao, J., Jin, X., Cheng, L., Wollenweber, S. D., & Manjeshwar, R. M. (2015). Quantitative comparison of OSEM and penalized likelihood image reconstruction using relative difference penalties for clinical PET. *Physics in medicine and biology*, 60(15), 5733–5751. <https://doi.org/10.1088/0031-9155/60/15/5733>.
20. Asma, E., Ahn, S., Ross, S.G., Chen, A., & Manjeshwar, R.M. (2012). Accurate and consistent lesion quantitation with clinically acceptable penalized likelihood images. 2012 IEEE Nuclear Science Symposium and Medical Imaging Conference Record (NSS/MIC), Anaheim, CA, USA, 2012, pp. 4062-4066, doi: 10.1109/NSSMIC.2012.6551928.
21. Ahn, S., & Fessler, J. A. (2003). Globally convergent image reconstruction for emission tomography using relaxed ordered subsets algorithms. *IEEE transactions on medical imaging*, 22(5), 613–626. <https://doi.org/10.1109/TMI.2003.812251>.
22. Reynés-Llompard, G., Gámez-Cenzano, C., Romero-Zayas, I., Rodríguez-Bel, L., Vercher-Conejero, J. L., & Martí-Climent, J. M. (2017). Performance Characteristics of the Whole-Body Discovery IQ PET/CT System. *Journal of nuclear medicine : official publication, Society of Nuclear Medicine*, 58(7), 1155–1161. <https://doi.org/10.2967/jnumed.116.185561>.
23. Hofheinz, F., Bütof, R., Apostolova, I., Zöphel, K., Steffen, I. G., Amthauer, H., Kotzerke, J., Baumann, M., & van den Hoff, J. (2016). An investigation of the relation between tumor-to-liver ratio (TLR) and tumor-to-blood standard uptake ratio (SUR) in oncological FDG PET. *EJNMMI research*, 6(1), 19. <https://doi.org/10.1186/s13550-016-0174-y>.
24. Sher, A., Lacoëuille, F., Fosse, P., Vervueren, L., Cahouet-Vannier, A., Dabli, D., Bouchet, F., & Couturier, O. (2016).

- For avid glucose tumors, the SUV peak is the most reliable parameter for [(18)F]FDG-PET/CT quantification, regardless of acquisition time. *EJNMMI research*, 6(1), 21. <https://doi.org/10.1186/s13550-016-0177-8>.
25. Viner, M., Mercier, G., Hao, F., Malladi, A., & Subramaniam, R. M. (2013). Liver SULmean at FDG PET/CT: interreader agreement and impact of placement of volume of interest. *Radiology*, 267(2), 596–601. <https://doi.org/10.1148/radiol.12121385>.
  26. Chilcott, A. K., Bradley, K. M., & McGowan, D. R. (2018). Effect of a Bayesian Penalized Likelihood PET Reconstruction Compared With Ordered Subset Expectation Maximization on Clinical Image Quality Over a Wide Range of Patient Weights. *AJR. American journal of roentgenology*, 210(1), 153–157. <https://doi.org/10.2214/AJR.17.18060>.
  27. Vallot, D., Caselles, O., Chaltiel, L., Fernandez, A., Gabiache, E., Dierickx, L., Zerdoud, S., Bauriaud, M., & Courbon, F. (2017). A clinical evaluation of the impact of the Bayesian penalized likelihood reconstruction algorithm on PET FDG metrics. *Nuclear medicine communications*, 38(11), 979–984. <https://doi.org/10.1097/MNM.0000000000000729>.
  28. Boellaard, R., Krak, N. C., Hoekstra, O. S., & Lammertsma, A. A. (2004). Effects of noise, image resolution, and ROI definition on the accuracy of standard uptake values: a simulation study. *Journal of nuclear medicine : official publication, Society of Nuclear Medicine*, 45(9), 1519–1527.
  29. Oliver, J. A., Budzevich, M., Hunt, D., Moros, E. G., Latifi, K., Dilling, T. J., Feygelman, V., & Zhang, G. (2017). Sensitivity of Image Features to Noise in Conventional and Respiratory-Gated PET/CT Images of Lung Cancer: Uncorrelated Noise Effects. *Technology in cancer research & treatment*, 16(5), 595–608. <https://doi.org/10.1177/1533034616661852>.
  30. Wahl, R. L., Jacene, H., Kasamon, Y., & Lodge, M. A. (2009). From RECIST to PERCIST: Evolving Considerations for PET response criteria in solid tumors. *Journal of nuclear medicine : official publication, Society of Nuclear Medicine*, 50 Suppl 1(Suppl 1), 122S–50S. <https://doi.org/10.2967/jnumed.108.057307>.
  31. Fuster, D., Duch, J., Paredes, P., Velasco, M., Muñoz, M., Santamaría, G., Fontanillas, M., & Pons, F. (2008). Preoperative staging of large primary breast cancer with [18F]fluorodeoxyglucose positron emission tomography/computed tomography compared with conventional imaging procedures. *Journal of clinical oncology : official journal of the American Society of Clinical Oncology*, 26(29), 4746–4751. <https://doi.org/10.1200/JCO.2008.17.1496>.
  32. Segaeert, I., Mottaghy, F., Ceyssens, S., De Wever, W., Stroobants, S., Van Ongeval, C., Van Limbergen, E., Wildiers, H., Paridaens, R., Vergote, I., Christiaens, M. R., & Neven, P. (2010). Additional value of PET-CT in staging of clinical stage IIB and III breast cancer. *The breast journal*, 16(6), 617–624. <https://doi.org/10.1111/j.1524-4741.2010.00987.x>.
  33. Yararbas, U., Avci, N. C., Yeniay, L., & Argon, A. M. (2018). The value of 18F-FDG PET/CT imaging in breast cancer staging. *Bosnian journal of basic medical sciences*, 18(1), 72–79. <https://doi.org/10.17305/bjbms.2017.2179>.
  34. Huyge, V., Garcia, C., Alexiou, J., Ameye, L., Vanderlinden, B., Lemort, M., Bergmann, P., Awada, A., Body, J. J., & Flamen, P. (2010). Heterogeneity of metabolic response to systemic therapy in metastatic breast cancer patients. *Clinical oncology (Royal College of Radiologists (Great Britain))*, 22(10), 818–827. <https://doi.org/10.1016/j.clon.2010.05.021>.
  35. Mosmann, M. P., Borba, M. A., de Macedo, F. P., Liguori, A. de A., Villarim Neto, A., & de Lima, K. C. (2016). Solitary pulmonary nodule and (18)F-FDG PET/CT. Part 1: epidemiology, morphological evaluation and cancer probability. *Radiologia brasileira*, 49(1), 35–42. <https://doi.org/10.1590/0100-3984.2014.0012>.
  36. Chen, S., Harmon, S., Perk, T., Li, X., Chen, M., Li, Y., & Jeraj, R. (2017). Diagnostic classification of solitary pulmonary nodules using dual time 18F-FDG PET/CT image texture features in granuloma-endemic regions. *Scientific reports*, 7(1), 9370. <https://doi.org/10.1038/s41598-017-08764-7>.
  37. Li, Z. Z., Huang, Y. L., Song, H. J., Wang, Y. J., & Huang, Y. (2018). The value of 18F-FDG-PET/CT in the diagnosis of solitary pulmonary nodules: A meta-analysis. *Medicine*, 97(12), e0130. <https://doi.org/10.1097/MD.00000000000010130>.
  38. Xia, Q., Feng, Y., Wu, C., Huang, G., Liu, J., Chen, T., Sun, X., Song, S., Tong, L., & Ni, Y. (2015). Differentiation between Malignant and Benign Solitary Lesions in the Liver with (18)FDG PET/CT: Accuracy of Age-related Diagnostic Standard. *Journal of Cancer*, 6(1), 40–47. <https://doi.org/10.7150/jca.10422>.
  39. Radan, L., Ben-Haim, S., Bar-Shalom, R., Guralnik, L., & Israel, O. (2006). The role of FDG-PET/CT in suspected recurrence of breast cancer. *Cancer*, 107(11), 2545–2551. <https://doi.org/10.1002/cncr.22292>.
  40. Cochet, A., David, S., Moodie, K., Drummond, E., Dutu, G., MacManus, M., Chua, B., & Hicks, R. J. (2014). The utility of 18 F-FDG PET/CT for suspected recurrent breast cancer: impact and prognostic stratification. *Cancer imaging : the official publication of the International Cancer Imaging Society*, 14(1), 13. <https://doi.org/10.1186/1470-7330-14-13>.
  41. Piva, R., Ticconi, F., Ceriani, V., Scalorbi, F., Fiz, F., Capitanio, S., Bauckneht, M., Cittadini, G., Sambucetti, G., & Morbelli, S. (2017). Comparative diagnostic accuracy of 18F-FDG PET/CT for breast cancer recurrence. *Breast cancer (Dove Medical Press)*, 9, 461–471. <https://doi.org/10.2147/BCTT.S111098>.
  42. Sampaio V. T et al., HPP Medicina Molecular SA, Porto; Lenitudes Medical Center & Research, Santa Maria da Feira, Aveiro; and School of Health Sciences, University of Aveiro, Aveiro, Portugal. *Clin Nucl Med*. 2017 Jul;42(7): e352 e354.



GE HealthCare

# It's time for a Theranostics revolution



**Cyclotron Solutions**  
PETtrace™ 800 Cyclotron  
<sup>68</sup>Ga Liquid Target  
<sup>68</sup>Ga Solid Target



**Radiochemistry**  
FASTlab™ 2 New  
Edition Developer



**Discovery PET/CT**  
Solutions with high sensitivity,  
Precision DL, Q.Clear & MotionFree  
to image <sup>68</sup>Ga for diagnosis,  
staging or restaging



**Digital SPECT/CT**  
Solutions to image and  
quantitate <sup>177</sup>Lu imaging  
accurately to personalise  
patient treatment



**Digital AI applications for**  
Effective quantitation  
including automatic  
**AI-based segmentation**

Discovery

Diagnosis

Treatment



**ESCO**  
HEALTHCARE



# Radiopharmacy Equipment

*The Ultimate Solution for Your Radiopharmaceutical Needs*



**Esco Frontier® Radioisotope™  
Fume Hood (EFI)**



**Cytoculture® Lead-Shielded  
Biological Safety Cabinet**



**Lead-shielded Biological  
Safety Cabinet**



**Streamline® Shielded  
Isolator**



**GMP-compliant Radioisotope  
Dispensing Isolator**



**Esco Philippines, Inc**  
Manila  
Unit 707E, 7th floor, East Tower Four E-com Center,  
Block 22 Seaside Cor Diokno Ave.  
MOA Complex, Pasay City 1300  
Tel: 0917 806 8026  
Email: [philippines@escolifesciences.com](mailto:philippines@escolifesciences.com)

**[www.escolifesciences.com](http://www.escolifesciences.com)**



PHILIPPINE SOCIETY OF NUCLEAR MEDICINE

# 41<sup>st</sup> ANNUAL CONVENTION

FEBRUARY 7-8, 2026 • BORACAY

*Save the date!*

*Celebrating  
60 years of PSNM*



# Biograph Trinion PET/CT

## Future-forward by design

[siemens-healthineers.com/en-ph/biograph-trinion](https://siemens-healthineers.com/en-ph/biograph-trinion)



Launch your future forward with a PET/CT that puts you confidently ahead of the curve and easily adapts to evolving clinical possibilities: Biograph Trinion™ with myExam Companion™.

Biograph Trinion PET/CT fully integrates best-in-class hardware and software to create one high-performance platform. A brand-new imaging experience puts patients more at ease, while users gain efficiency from a modern design and AI-supported workflow. Always the right fit, Biograph Trinion provides a sustainable investment from today onward—delivering reduced costs through its compact footprint, automated energy-saving features, and on-site scalability.

**SIEMENS**  
**Healthineers**

**Symbia Pro.specta SPECT/CT  
with myExam Companion**

# Modernize to MAXIMIZE



**Take your nuclear medicine department into the future with intelligent SPECT/CT imaging. Symbia Pro.specta™ with myExam Companion™ gives you the power of more.**

## **Redefine performance with new standards for SPECT/CT**

Automatic SPECT motion correction and up to 64-slice CT enable faster scanning at the highest image quality.<sup>1</sup>

## **Reach your full potential with a smart workflow**

A single, intuitive interface automates steps across the entire workflow—helping you achieve high-quality, reproducible results.

## **Achieve optimized imaging from dedicated clinical tools**

A multi-purpose SPECT/CT that transforms into a specialized camera for cardiology, neurology, oncology, theranostics, and more.

<sup>1</sup> Based on competitive literature at time of publication. Data on file.

Symbia Pro.specta SPECT/CT is not commercially available in all countries. Future availability cannot be guaranteed. Please contact your local Siemens Healthineers organization for further details.

Learn more at [siemens-healthineers.com/symbia-prospecta](https://siemens-healthineers.com/symbia-prospecta)

**SIEMENS**  
**Healthineers**